Heliyon 10 (2024) e34183

Contents lists available at ScienceDirect

Heliyon

journal homepage: www.cell.com/heliyon

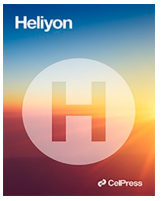

Research article

Insights on the comparative affinity of ribonucleic acids with plant-based beta carboline alkaloid, harmine: Spectroscopic, calorimetric and computational evaluation

Paromita Sarkar [a], Priyanka Gopi [b,1], Prateek Pandya [b,1], Samaresh Paria [c,1], Maidul Hossain [c,1], Manzer H. Siddiqui [d], Saud Alamri [d], Kakali Bhadra [a,*]

[a] University of Kalyani, Department of Zoology, Nadia, W. Bengal, 741235, India
[b] Amity Institute of Forensic Sciences, Amity University, Noida, Uttar Pradesh, India
[c] Vidyasagar University, Department of Chemistry, Midnapore 721 102, West Bengal, India
[d] Department of Botany and Microbiology, College of Science, King Saud University, Riyadh, Saudi Arabia

ARTICLE INFO

Keywords:
Harmine
Beta-carboline alkaloid
Ribonucleic acids RNAs
Molecular docking
Molecular dynamics
Principal component analysis (PCA)
Isothermal calorimetry
Spectroscopy

ABSTRACT

Small molecules as ligands target multifunctional ribonucleic acids (RNA) for therapeutic engagement. This study explores how the anticancer DNA intercalator harmine interacts various motifs of RNAs, including the single-stranded A-form poly (rA), the clover leaf $tRNA^{phe}$, and the double-stranded A-form poly (rC)-poly (rG). Harmine showed the affinity to the polynucleotides in the order, poly (rA) > $tRNA^{phe}$ > poly (rC)·poly (rG). While no induced circular dichroism change was detected with poly (rC)poly (rG), significant structural alterations of poly (rA) followed by $tRNA^{phe}$ and occurrence of concurrent initiation of optical activity in the attached achiral molecule of alkaloid was reported. At 25 °C, the affinity further showed exothermic and entropy-driven binding. The interaction also highlighted heat capacity (ΔC_p^o) and Gibbs energy contribution from the hydrophobic transfer (ΔG_{hyd}) of binding with harmine. Molecular docking calculations indicated that harmine exhibits higher affinity for poly (rA) compared to $tRNA^{phe}$ and poly (rC)·poly (rG). Subsequent molecular dynamics simulations were conducted to investigate the binding mode and stability of harmine with poly(A), $tRNA^{phe}$, and poly (rC)·poly (rG). The results revealed that harmine adopts a partial intercalative binding with poly (rA) and $tRNA^{phe}$, characterized by pronounced stacking forces and stronger binding free energy observed with poly (rA), while a comparatively weaker binding free energy was observed with $tRNA^{phe}$. In contrast, the stacking forces with poly (rC)·poly (rG) were comparatively less pronounced and adopts a groove binding mode. It was also supported by ferrocyanide quenching analysis. All these findings univocally provide detailed insight into the binding specificity of harmine, to single stranded poly (rA) over other RNA motifs, probably suggesting a self-structure formation in poly (rA) with harmine and its potential as a lead compound for RNA based drug targeting.

* Corresponding author.
E-mail addresses: sarkarparomita13@gmail.com (P. Sarkar), priyankagopi5495@gmail.com (P. Gopi), ppandya@amity.edu, prateekpandya@gmail.com (P. Pandya), samarchemistry96@gmail.com (S. Paria), hossainm@mail.vidyasagar.ac.in (M. Hossain), mhsiddiqui@ksu.edu.sa (M.H. Siddiqui), saualamri@ksu.edu.sa (S. Alamri), kakali_bhadra2004@yahoo.com, *kakalibhadra3@gmail.com* (K. Bhadra).
[1] PG, SP, MH & PP: *All contributed equally*.

https://doi.org/10.1016/j.heliyon.2024.e34183
Received 14 March 2024; Received in revised form 4 July 2024; Accepted 4 July 2024
Available online 5 July 2024

1. Introduction

Only 0.05 % of the human genome is targeted by small molecules and antibody treatments, and the majority of diseases target lack well-defined active regions that small molecules may bind to. The spectrum of druggable targets is widened by abundant RNAs' selective action on proteins, transcripts, and genes. Recently, development of RNA treatments is greatly facilitated by a standard sequence for RNA targeted drugs [1]. RNA therapy that refers to the treatment or prevention of diseases using RNA-based molecules, has rich history, various applications and unlimited future prospects [2]. Lately, list of altered miRNAs and long noncoding RNAs (lncRNAs), their targeted genes, and pathway analysis were performed for pancreatic carcinogenesis [3–6]. Therefore, the focus has been shifted from DNA targeted molecules to RNA binding molecules. Several RNA drugs have been authorized, and another dozen are under trials to treat common and uncommon disorders [1].

RNAs are incredibly adaptable molecules that have been connected to a variety of biological functions along with development of numerous diseases caused by viruses [7–9]. Moreover, it plays significant function in accelerating the progress of novel antibiotics targeting bacterial rRNA [10]. Discovery of micro RNAs with their contribution in biological functions further augmented the significance of RNAs [11–13]. Numerous dsRNAs, tRNAs, and mitochondrial introns play key roles as bio-markers in microbial ecology and in the splicing of pre-mRNA, the solubility of C5 protein inside cells, silencing of particular genes and the production of self-splicing RNA molecules [14–18]. Hence study of various RNA conformations including intricate tertiary and secondary motifs, in-trans and cis conformations and its targeting drug molecules is very significant in research. Numerous man-made and natural compounds have been found to be carcinogens or mutagens [19]. Although these don't directly interact with nucleic acids *in vivo*, metabolic processes change them to produce electrophiles that form covalent bonds with DNA, RNA, or even proteins. The enzyme known as mixed-function cytochrome P-450 oxidase, whose primary role appears to be the detoxification of foreign compounds, is responsible for the majority of these changes [19]. While in non-covalent reversible interactions, modes of binding of the therapeutic molecules to the nucleic acids occurs in two steps: the first step occurs outside the helix, while the second step accounts for intercalation with concurrent helix unwinding, lengthening, and overall stiffness [20,21]. DNA polynucleotides show intercalative, partial intercalative and groove binding based on the structure of the drug molecule [22–24]. Similarly, RNAs also show the above mode of binding with the various drug molecules based on the varied motifs of the polynucleotides and structure of the drug molecules [25–27]. The rational design of novel RNA binding drugs require a thorough understanding of the binding mode, mechanism, affinity, specificity, and selectivity of already existing drugs. These parameters can only be discovered by investigating the interactions of known compounds with known RNA structures. In the creation of RNA targeted therapeutics, one method has been to create a database on the interactions of already known DNA binding compounds in order to investigate how they might specifically recognize the RNA conformations.

The extracts of many natural products have been reported to possess antitumor effect [28–34]. One such product is *Peganum harmala* that had been used for many years in traditional medicine in many regions of the world mainly in Middle east and China. Apart from *Peganum harmala*, beta carboline compounds also exist in other medicinal plants and mammalian tissues. In *P. harmala* extracts, harmine and harmaline made up more than 70 % of the composition [35]. Harmine, an unsaturated fully aromatic β-carboline alkaloid, has been described by the author to possess antitumor properties and was tested for cervical cancer therapy [36]. Harmine has been reported to enhance the activity of the HIV-1 latency-reversing agents ingenol A and SAHA [37]. Additionally, harmine along with few other isoquinoline alkaloids have been found to have therapeutic potential for myotonic dystrophy type I [38]. According to earlier research, harmine suppresses the growth and triggers death in a variety of tumor cell types via a number of signaling methods [39–41]. Even though there are many reports about the binding of β-carboline compounds with deoxyribonucleic acids [42–46], not much information is obtainable about their binding and affinity with different conformational structures of ribonucleic acid RNA [47–49]. Actually, it is the detrimental influence on DNA that has been a frequently studied area that aids carcinogenesis, the development of genetic disorders and cancer. Whereas because of our limited knowledge of RNA structures and its functional behavior,

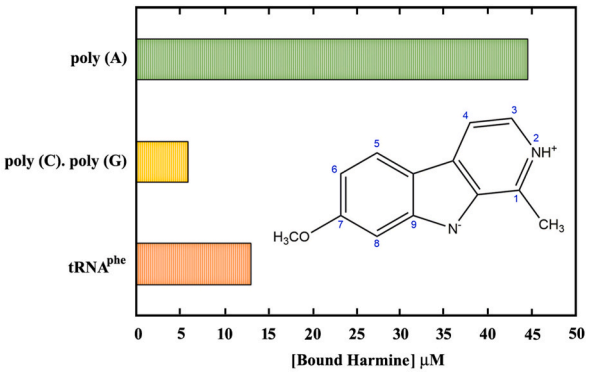

Fig. 1. Competition dialysis analysis at 25 ± 0.5 °C in 15 mM citrate-phosphate buffer with pH 6.8. A bar graph representing the amount of harmine bound to each sample of RNA polymer is displayed. The statistics shown are the average results of four different tests conducted in the same manner. Inset: Structure of harmine.

even today's probable causes of RNA damage are still at a basic level.

This research focused to explain the binding of harmine (Fig. 1, inset), with different structural motifs of RNA *viz*. poly (rA), poly (rC)·poly (rG) and $tRNA^{phe}$ based on calorimetric, multifaceted spectroscopic, and in-silico approaches. All the three polynucleotides are biologically and structurally very significant. Attention has been drawn to polyriboadenylic acid poly (rA) because of its significance in mRNA functioning [20,50,51]. Poly (rA) has the unique characteristics to exist either as a single stranded helix or as a parallel stranded double helical structure. These structures have been fully characterized [20,52,53], the latter being stabilized by base paired protonated adenines. Many small molecules, mostly alkaloids, have been shown to induce a unique self-assembled structure formation in poly(A), similar to the low pH induced bihelix [26,54,55]. Unilike poly (rA), under natural conditions, poly (rC)-poly (rG) assumes a double-stranded A-form structure [25]. Efficacious interferon induction (IFN) and double-stranded RNAs' antiviral properties have been reported [56,57]. Bovine enteroviruses, encephalomyocarditis virus, and foot-and-mouth disease viruses all feature sequences of C-G double-stranded RNA structures in their genomes [58]. On the other hand, the most adaptable, soluble natural RNA molecules are tRNAs, which have a clover leaf structure with significant folding that is maintained via base stacking, base pairing, and other tertiary interactions [20]. By decoding the message contained in nucleic acids (nucleotides) and translating it into proteins (amino acids), tRNA attaches to the ribosomal A-site which is a vital component of the translation process. There have been several studies in comprehending tRNA-small molecules binding [59–61]. The originality of the present study results from the conformational and structural aspects towards possible disorders imposed on ribonucleic acid structures on account of interaction with harmine, which may be associated to RNAs cellular dysfunction. This would increase our understanding in designing RNA targeted drugs for future therapeutic purposes.

2. Materials and methods

2.1. Apparatus

Jasco V-630 monochromator double-beam spectrophotometer (Jasco International Co. Ltd, Tokyo) attached with a thermo-electrically controlled cell holder in matched quartz cells of 1 cm path length under stirring at 25 ± 0.5 °C was utilized for measuring the absorbance spectra. The above unit with Jasco PAC-743 accessory attachment, was used for analyzing the melting curves [45]. Quartz cells with a 1 cm path length for the steady state fluorescence measurements on a Hitachi F-7000 fluorescence spectrometer were used. The excitation wavelength for harmine was 376 nm [36]. Excitation and emission band passes were kept to 2.5 and 10 nm for all experimental measurements. The sample was kept at a constant temperature of 25 ± 0.5 °C. Jasco J-1500 CD spectrometer equipped with a temperature programmer (model PFD 425 L/15) and temperature controller, was used to record CD spectra. Isothermal titration calorimetry (ITC) experiments were performed by Nano ITC, TA instruments, independent model [62,63]. Differential scanning calorimetry, DSC, was studied on a Microcal VP-differential scanning calorimeter (MicroCal, Inc., Northampton, MA, USA) and analyzed using Origin 7.0 software [62].

2.2. Materials

Harmine was procured from Sigma-Aldrich in St. Louis, Missouri, USA. The sample's purity was verified in the manner specified previously [36]. The alkaloid concentration was calculated using molar absorption coefficient (ε) of 14,600 M^{-1} cm^{-1} at 318 nm [39]. Poly (rC). poly (rG), $tRNA^{Phe}$ (yeast) and poly (rA) were also acquired from Sigma. Using a molar absorption coefficient (ε) of 10,000 M^{-1} cm^{-1} at 257 nm, 7700 M^{-1} cm^{-1} at 259 nm and 6900 M^{-1} cm^{-1} at 260 nm, for poly(A), poly (rC). poly (rG) and $tRNA^{Phe}$ (yeast) respectively, at neutral pH buffer, spectrophotometric analysis was used to determine the concentration of these polynucleotides [62,63]. Nucleotide phosphates were used to express all concentrations of the polynucleotides. It was citrate-phosphate (CP) buffer (15 mM [Na^+]), pH 6.8 where the experiments were conducted for the binding of harmine to poly (rC). poly (rG) and poly (rA). For binding studies with $tRNA^{Phe}$, additional 3 mM $MgCl_2$ was added to the CP buffer [64,65]. To get rid of any impurities, the buffer solutions, made in MilliQ water, were run through 0.45 μm syringe filters (Millipore India Pvt. Ltd. In Bengaluru, Karnataka). All other chemicals and reagents were of analytical grade.

2.3. Methods

2.3.1. Assay by competition dialysis

The protocol of competition dialysis assay was followed based on protocol developed by Chaires [48]. Origin 7.0 software (Micro Cal, Inc., CA, USA) was used to plot the data in the form of bar graph. This data was then used to compute the apparent binding constant (K_{app}) using the relation

$$K_{app} = C_b/\ (C_f)\ (S_{total} - C_b) \quad (1)$$

2.3.2. Quantum efficiency by fluorescence spectroscopy

Analysis of quantum yield using the Parker and Rees equation (3) were performed as mentioned previously [63] by Hitachi F-7000 with specific parameter settings of -excitation wavelength: 318 nm; emission start wavelength: 350 nm; emission end wavelength: 600

nm; scan speed: 1200 nm/min; excitation slit:2.5 nm; emission slit: 5.0 nm; PMT Voltage: 600 V; response: 0.5 s.

$$\varphi_s = (F_s \varepsilon_q C_q \times 0{:}55) \,/\, (\mathrm{Fq} - \varepsilon_s C_s) \quad (2)$$

Where ε represents the molar extinction coefficient, C represents the molar concentration of sample (s) and quinine sulfate (q) and F is the integrated area of the fluorescence emission curve in arbitrary unit. For measurements of quantum yield, quinine sulfate in 0.1 N H_2SO_4 was used as the reference standard.

2.3.3. Ferrocyanide quenching analysis

The anionic quencher $[Fe(CN)_6]^{4-}$ was used in the quenching technique analysis. The experiments were executed by mixing KCl, and K_4 $[Fe(CN)^6]$ at fixed total ionic strength, in addition to the normal buffer components. Fluorescence quenching studies were carried out at a fixed P/D (nucleotide phosphate/alkaloid molar ratio), detecting the change in fluorescence intensity as a function of increasing ferrocyanide concentration as outlined earlier [27,66]. Each set received an average of at least four measurements. Stern–Volmer plots of F_o/F versus ferrocyanide ion concentration were plotted.

2.3.4. Circular dichroism (CD) studies

Conformational alterations in the intrinsic CD regions (210–400 nm) were checked with a fixed RNA concentration of 65 μM titrated with an increasing concentration of the alkaloid harmine in a 1 cm path length of cuvette as described earlier [43–45]. Equipment settings were: band-width of 1.0 nm, scan rate of 100 nm/min, sensitivity of 100 m degree response time of 1 s and no of scans = five. It was in terms of per nucleotide phosphate that the molar ellipticity [θ] values in the spectra were plotted.

2.3.5. Isothermal calorimetry (ITC) analysis of RNAs binding to harmine

Aliquots of degassed polynucleotide solutions (1000 μM) were injected into the isothermal sample chamber with the alkaloid (10 μM) solution using a revolving syringe at 290 rpm. Control experiments were performed by injecting identical volumes of the same (corresponding polynucleotide) into the buffer to analyze the heat of dilution. The time interval of each injection was 10 s and the delay time between each injection was 180 s. An initial delay of 60 s was maintained before the first injection. Each injection of 10 μL produced a heat burst curve (microcalories per second versus time). The heat associated with each alkaloid-buffer mixing was subtracted from the consistent heat related with the polynucleotide injection to the alkaloid to give the heat of alkaloid binding to the polynucleotide. The resulting corrected heat injection were plotted as a function of the P/D [nucleotide phosphate molar ratio]/[alk], fit with a model for one set of binding sites, to analyze the binding affinity (K_b), the binding stoichiometry (N) and the enthalpy of binding (ΔH^o). The free energies (ΔG^o) were determined using the standard relationship

$$\Delta G^o = -\mathrm{RT} \ln K_b \ldots\ldots\ldots\ldots\ldots\ldots\ldots\ldots\ldots \quad \ldots(3)$$

Where temperature T in Kelvin (293.15 K) and the gas constant R (1.987 cal. K^{-1} mol^{-1}). The binding free energy along with the binding enthalpy gave the value of the entropic contribution ($T\Delta S^o$), where ΔS^o is the calculated binding entropy, using the standard equation

$$T\Delta S^o = \Delta H^o - \Delta G^o \ldots\ldots\ldots\ldots\ldots\ldots\ldots\ldots\ldots\ldots \quad (4)$$

Three times each experiment was repeated, and the error value, which reflects the standard deviations between the several runs, was never greater than 10 %.

2.3.6. In-silico analysis

2.3.6.1. Molecular docking. AutoDock 4.2 software [67] was employed to perform molecular docking calculations of Harmine (HRM) with poly (rA) (PA), poly (rC). poly (rG) (PGC) and tRNA (TRNA) to evaluate the binding mode and affinity. The crystal structure of TRNA (PDB ID: 6UGG) with a resolution of 1.95 Å was obtained from Protein Data Bank [68], while the 3D structures of PA and PGC was created and minimized using Biovia Discovery Studio. The 3D structure of HRM was procured from PubChem and converted to PDB using Biovia Discovery Studio [69]. To rectify any changes in the geometries, charges and valences, minimization of HRM, PA, PGC and TRNA were performed on Avagadro software by using the steepest descent and conjugate gradient protocols and MMFF94 force field [70,71]. To facilitate the docking procedure, AutoDock Tools 1.5.6 [67] was utilized for the creation of receptor map files and the generation of grid and docking parameters. A grid spacing of 0.375 Å was used to cover the entire receptor encompassing all the domains of TRNA and grooves of PA and PGC [48,49]. A total of 100 poses were generated for each rigid docking calculation with a set energy evaluation of 25000000 for every step.

2.3.6.2. Molecular dynamics. NAMD GPU 2.0 [72] on Google Colab platform was used to perform molecular dynamics simulations of the receptor-ligand systems. We examined the docked position with the lowest binding affinity as the starting structure for the simulations. To generate topology and parameter files for the receptor and ligand molecules, CHARMM GUI [68,73] was employed, and the resulting complexes were solvated using the TIP3P water model. To neutralize the complex systems, appropriate sodium and chloride ions were added, and the complex systems were minimized for 8000 steps. The salt concentrations for Poly-A, Poly-dC and tRNA was 15 mM $[Na^+]$ with an additional 3 mM $MgCl_2$ for tRNA (for maintaining the tertiary structure), while maintaining a constant pH of 6.8. The chain lengths of Poly-A and Poly-dC were set to 10 nucleobases and 12 base pairs in our study to complete one helical

turn in a duplex. The dcd freq, xst freq, output energies and restart freq were all set to 2000, while the switch dist, cutoff and pair dist list were set to 11, 12, and 13 respectively. The timestep was set to 2 and steps per cycle were set to 20. Langevin Piston was on with the Target set to 1.02 atm for a period of 150 and decay set to 90. The PBC conditions were throughout maintained the simulations with the water wrapped to the central cell. SHAKE algorithm was not used for the production run. Both NVT and NPT equilibrations were performed for 1ns each followed by a production run of 100ns for all complexes [74–77]. The simulations were performed on the set parameters of 298K temperature and 1.02 atm pressure using CHARMM36 force fields [78–81]. Despite its limitations, CHARMM36 remains one of the most reliable force fields available for RNA simulations [78–81], making it a suitable choice for our study. Analysis

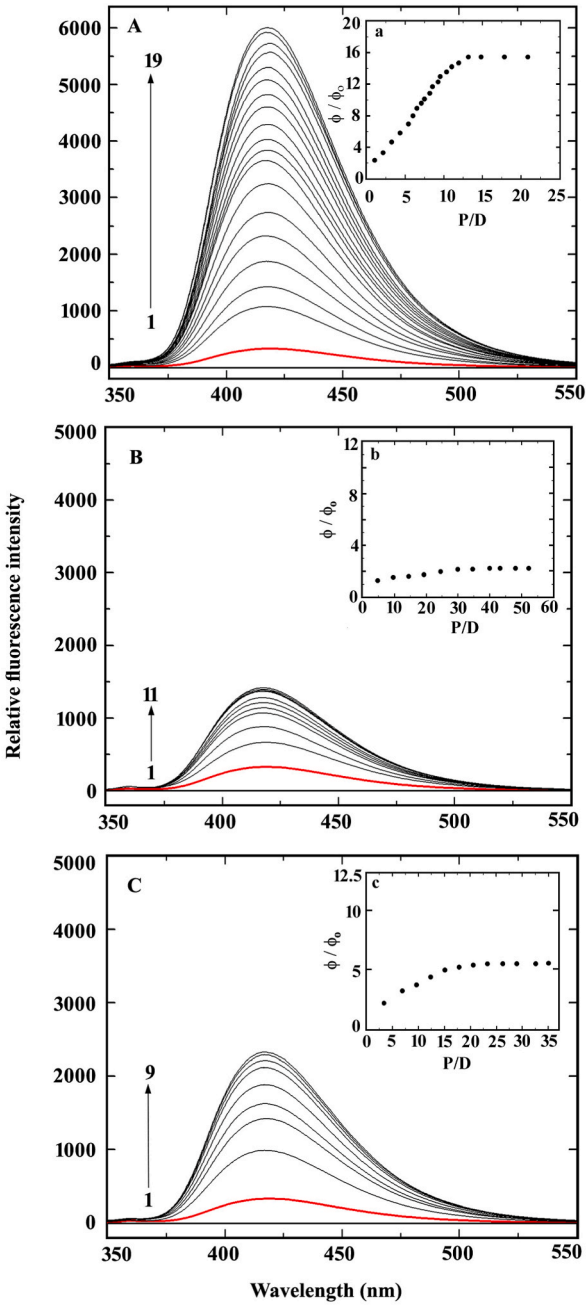

Fig. 2. Representative steady state fluorescence emission spectral changes of harmine (3 μM, Curve 1) treated with (A) 2.0, 3.5, 4.0, 5.8, 10.6, 12.5, 15.5, 18.0, 20.6, 22.5, 25.0, 27.0, 30.0, 31.5, 32.4, 33.5, 35.0 and 36.0 μM (curves 2–19) of Poly (rA), (B) 10.0, 20.05, 30.7, 47.5, 55.5, 65.0, 75.0, 85.6, 105.5 and 120.0 μM (curves 2–11) of poly (rC)·poly (rG) and (C) denote 5.0, 10.2, 15.9, 30.5, 40.7, 58.6, 65.0, and 75.0 μM (curves 2–9) of tRNAphe in 15 mM CP buffer, pH 6.8 at 25 ± 0.5 °C. Inset of A, B, and C represent plots of the relative quantum yield φ/φo vs. P/D for the interaction of harmine (●) with the respective RNA nucleotides.

of all trajectories including RMSD, Rg and Bonds were evaluated on VMD 1.9.3 software [82]. Additionally, eRMSD was calculated to measure the deviation of the receptor structure from its ideal native conformation using Barnaba software.

2.3.6.3. Principal Component Analysis (PCA). Furthermore, Principal Component Analysis (PCA) was computed on the MD trajectories to assess the ligand induced conformational variations on the receptors by using the Bio3d package [83], a component of the R statistical interface on Galaxy Cheminformatics Server [84]. The eigenvectors, eigenvalues, and their projection along the first three principal components were analyzed [85]. Eigenvectors provide insight into the direction of the motion and fluctuation of the polymers, while eigenvalues convey the amplitude of these motions [86]. PCA captures the most pronounced and variable dynamic motions within simulations, which are crucial for biological functionality [87]. Drug-bound complexes in a stable state will exhibit diminished dynamic fluctuations due to the site's rigidity induced by the binding of the drug/ligand [86,87].

2.3.6.4. MM/PBSA. For the calculation of binding free energies in all the complexes, the MM/PBSA (Poisson Boltzmann Surface Area) method was employed [88]. This approach combines gas phase free energy (molecular mechanics) with polar and non-polar solvation energies to estimate binding free energies. To perform these calculations, 2500 stable snapshots were extracted from the trajectories obtained during the 100 ns simulations of HRM complexes with PA, PGC, and TRNA. 2500 stable snapshots were extracted from every 20 ps after the 25 ns marked in our analysis. The MM/PBSA calculations were carried out using the gmx_MMPBSA tool [89].

3. Results and discussion

3.1. Competition dialysis assay

Competition dialysis assays are used to find ligands that can bind to nucleic acids with structural and sequence selectivity. They are based on the thermodynamic theory of equilibrium dialysis and was developed by Chaires [90]. The result showed that at equilibrium, more harmine (Fig. 1 inset) collects in the RNA containing dialysis tube to which it has the maximum binding. Based on the outcomes of the experimental results, bound harmine was 44.66 μM in the dialysis tube of poly (rA) followed by 12.98 μM in the dialysis tube containing $tRNA^{phe}$ and least amount of 5.85 μM in the dialysis tube with poly (rC)·poly (rG) (Fig. 1). K_{app} was obtained from the experimental results, where the corresponding values were found to be $4.24 \pm 0.01 \times 10^5$, $0.947 \pm 0.004 \times 10^5$ and $0.243 \pm 0.002 \times 10^5$ M^{-1}, for poly (rA), $tRNA^{phe}$ and poly (rC)·poly (rG), respectively. So, harmine had the highest binding affinity for single-stranded poly (rA), followed by cloverleaf $tRNA^{phe}$, and the lowest binding affinity for double-stranded poly (rC)poly (rG).

3.2. Spectroscopic results and estimation of binding parameters

Harmine gives fluorescence peak at 417 nm, when excited at 318 nm. Fluorescence emission spectra of the alkaloid on titration with ribonucleic acids were studied in the range of 350–450 nm (Fig. 2A–C). Harmine fluorescence was gradually enhanced while titrating with increasing concentration of the RNA polymers, finally attaining the peak of saturation. The fluorescence increase was greatest with poly (rA), then $tRNA^{phe}$, and least in poly (rC)-poly (rG). Quantum yield (φ/φ_o) data were analyzed based on fluorescence titration (inset, Fig. 2A–C) and the values were presented in Table 1 φ/φ_o analysis showed 16.35 ± 0.6 at saturation P/D 12 with harmine-poly (rA), while harmine-$tRNA^{phe}$ gave φ/φ_o of 5.72 ± 0.04 at saturation P/D 25 and harmine-poly (rC)·poly (rG) showed φ/φ_o of 2.55 ± 0.03 at saturation P/D 40. Fluorescence intensity at 417 nm *vs* concentration of the free alkaloid molecule was checked (Fig. S1).

To further study the interaction phenomena of harmine with the above RNA polymers, Benesi Hildebrand plot was used by UV absorption spectroscopic technique (91–93). The absorption spectra of harmine (10 μM) in presence of increasing RNA polynucleotide concentrations are presented in Figs. S2A–C. During the experiment, RNA was added both in the sample and reference cell. So, the contribution of the RNA gets automatically nullified. The titration showed hypochromic and negligible (~1.00 nm) bathochromic shifts. No clear isosbestic point was observed, which may be due to the fact that the molar extinction coefficient of harmine-RNA complex is very much lower than that of the alkaloid alone or may be indicative of more than one type of binding [94]. But, the absorbance spectra of harmine showed a pronounced hypochromic effect with increasing concentration of RNA polymers suggesting a strong association of the alkaloid to RNAs. The hypochromic changes were more in poly (rA) followed by $tRNA^{phe}$ and least with poly

Table 1
Spectrofluorometric analysis of comparative quantum yield and K_4 $[Fe(CN)_6]$ quenching constant obtained from the RNA- Harmine complex in 15 mM CP buffer at 250C.

RNA polymers	Spectrofluorimetric analysis		
	φ/φ_o at saturation P/D	K'_{sv} M^{-1} (free alkaloid)	K'_{sv} M^{-1} (bound alkaloid)
poly (rA)	16.35 ± 0.6	314 ± 7	149 ± 4
poly (rC)·poly (rG)	2.55 ± 0.03	314 ± 7	246 ± 6
t-RNA^{phe}	5.72 ± 0.04	314 ± 7	201 ± 6

[a]Data is expressed based on an average of four determinations made for each. φ/φ_o denotes the relative quantum yield value at saturation nucleotide/alkaloid molar ratio (P/D) determined as described in the text. Spectrophotometry analysis by Benesi Hildebrand plot for binding constant K_i has been presented in Fig, S2.

(rC)·poly (rG). Binding parameters (inset, Fig. S2 A-C) from the absorption titration, evaluated by Benesie-Hildebrand plot showed preference and binding affinity of harmine with the above polynucleotides [91–93,95]. However, in the UV spectroscopy with an isosbestic point in the spectra because of binding, McGhee and vonHippel Scatchard analysis may be applied [22–27,43,44,48,49].

3.3. UV optical thermal melting study

The optical thermal melting of nucleic acid-drug complexes is a useful approach for studying interaction and stabilization by the small molecules. The neutralisation of phosphate charges of the polynucleotides via external binding, as well as the stacking interactions of intercalated or partial intercalated molecules, all contribute to an increase in melting temperature. Absorbance versus temperature profiles (melting curves) of the three polynucleotides *viz.* poly (rA), $tRNA^{phe}$ and poly (rC)·poly (rG) were measured on the Jasco PAC-743 accessory attachment (Fig.S3 A-C).

The free poly (rA) (curve 1, Fig.S3 A) melting profile revealed a wide non-cooperative transition with no acute UV melting temperature. However, with harmine, a cooperative melting transition was observed (curve 2, Fig.S3 A), indicating that the alkaloid induced self-structure in poly (rA). The thermal melting of poly (rA) with different harmine input ratios revealed that at D/P [alk]/[nucleotide phosphate molar ratio] 0.5, poly (rA) cooperatively melts with a T_m of 65 ± 1 °C. The melting of the cloverleaf $tRNA^{phe}$ structure in the absence of harnime revealed transitions at 36 ± 1, 49 ± 1 and 65 ± 1 °C (curve 1, Fig.S3 B). The averaged melting temperature of the $tRNA^{phe}$ is about 48 ± 1 °C [96,97]. In presence of harmine at D/P 0.6, the average T_m of tRNA increased by 4 ± 1 °C (Curve 2, Fig.S3 B). The melting curve demonstrated a cooperative transition with a hyperchromicity change that spanned the temperature range. The A-form double stranded poly (rC)poly (rG) structure, on the other hand, is astonishingly stable and does not melt under our solution conditions until 110 °C (Curve 1, Fig.S3 C), the limit of the UV-melting equipment [25,98].

3.4. Ferrocyanide quenching analysis

Fluorescence spectroscopy was also used for fluorescence quenching study that serves as a definitive method to probe the availability of the alkaloid molecule to fluorescence quencher like ferrocyanide ion $[Fe(CN)_6]^{4-}$. Due to the electrostatic barrier created by the negatively charged phosphate groups, an anionic quencher like the $[Fe(CN)_6]^{4-}$ ion will not be able to penetrate the inside of the helix, and as a result, very little quenching will be seen in the case of compounds bound inside the helical RNA. When compared to intercalation, the ligand/alkaloid binding to the grooves is exposed to the solvent to a higher extent, making it more accessible to the quencher. On calculation, the values of Stern-Volmer quenching constants for free harmine (314 ± 7 M^{-1}) and its complexes were, 149 ± 4, 246 ± 6 and 201 ± 6 M^{-1} with poly (rA), poly (rC).poly (rG) and $tRNA^{phe}$, respectively (Table 1; Fig. 3).

Consequently, the magnitude of the Stern–Volmer quenching constant (K_{sv}) of ligands that are bound inside will be less than that of the unbound molecules. The site of the attached alkaloid molecule is suggested to be partially sequestered from the solvent by the inference of the Stern-Volmer quenching constant values, pointing towards a partial intercalation approach of binding to poly (rA) followed by $tRNA^{phe}$. As the alkaloid showed different percentage of quenching with the polynucleotides, it can be inferred that harmine approached the polynucleotides in different fashion which largely depends on the latter's conformation mainly and also on the sequence of base-pairs. Furthermore, the orientation of base pairs, electrostatic charges on them may also influence the mode of binding. Thus, the nature of binding for the alkaloid become apparent from ferrocyanide ion quenching studies - partial intercalation to poly (rA) and $tRNA^{phe}$ while weak intercalation to poly (rC).poly (rG). The proposed mode of binding from the above analysis has been

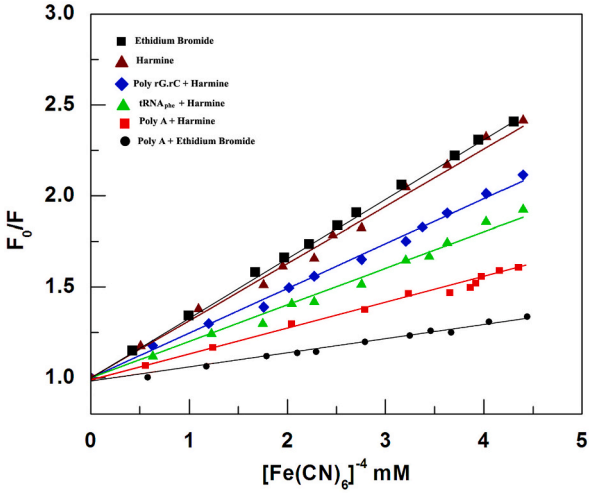

Fig. 3. Stern-Volmer plots for quenching by increasing concentration of $[Fe(CN)_6]^{-4}$ with harmine in the absence and presence of respective polynucleotides represented by different symbols in the figure. The plots have been compared with ethidium bromide, as classical intercalator. The corresponding K'_{sv} values are presented in Table 1.

further confirmed from docking and dynamic simulation (*vide infra*).

3.5. Secondary structural changes in RNA conformation

Differences in the chiral confirmation of RNA polynucleotides due to alkaloid-RNA interactions can be analyzed with the help of circular dichroism (CD) spectroscopy [43,44,62,96,98]. Additionally, it provides detail evidence on how the orientation of the ligand chromophore happened inside the helical conformation of the adjacent nucleic acid base pairs that happened because of some asymmetric (chiral) electronic interactions of $\pi \rightarrow \pi^*$ at the interactive site due to ligand-nucleic acid non-degenerative coupling [43,44,49,62,97,99]. The region 215–550 nm was chosen to monitor the structural perturbations of the RNA structures as non-covalent interactions with harmine that subsequently alter the intrinsic CD spectral behavior of the RNA polynucleotides. The spectra 1 of Fig. 4 A-C are the CD representation of the RNA polynucleotides, poly (rA), poly (rC).poly(G) and $tRNA^{phe}$, respectively, displaying the conventional conformations of the polymers. Binding of harmine with poly (rA) showed slight perturbation in the 265 nm positive peak, while the 250 nm negative peak showed prominent changes in molar ellipticity. An extrinsic CD positive broad band from 350 to 450 nm and negative band from 450 to 525 nm was observed with an isodichroic point at 450 nm which corroborates again a strong affinity where the bound and unbound molecules are in equilibrium. Harmine with poly (rC).poly (rG) on the other hand showed a weak interaction with no extrinsic CD bands. While, binding of harmine with $tRNA^{phe}$ showed a decrease in peak in the UV region at 272 nm. Along with this modification, a positive induced CD band with increasing ellipticity in the band region 465–525 nm wavelengths also developed as the binding progressed. Consequently, CD modifications offered a means to display the distinct binding positions of harmine with the different conformational structures of RNA polynucleotides.

3.6. Calorimetric analysis by isothermal titration calorimetry (ITC)

Isothermal calorimetry is a consistent and reliable approach for the precise measurement of thermodynamic parameters in various biomolecular interactions by offering important understandings of the chemical mechanisms behind complex formation [100–105]. The complete thermodynamic profile like the entropy contribution ($T\Delta S^o$), Gibbs energy change (ΔG^o), binding enthalpy (ΔH^o), and also the stoichiometry (N) and binding affinity (K) can be provided by ITC [106,107]. Every single injection is indicated by each heat burst curve in upper panel of Figs. S3 and S4. The injection is obtained by integrating the areas within this heat burst curves. These injection heats are adjusted by deducting the appropriate dilution heats obtained from injecting identical volumes of macromolecule (RNA polynucleotides) into buffer alone. The resulting adjusted injection heats are represented against the relevant molar ratios and are presented at the bottom panel of the graphs, whereas, the solid line provides calculated best-fitted line of the data. Table 2 summarizes the calorimetric data. Fig. 5A–C shows the binding affinity values of harmine with poly (rA), poly (rC).poly (rG) and $tRNA^{phe}$, respectively evaluated at 25 ± 0.5 °C. The bindings are exothermic and entropically driven. A K_b value of $1.22 \pm 0.04 \times 10^6$ M^{-1} with a stoichiometry of 4.08 nucleotide phosphates was obtained by harmine interacting with poly (rA). In addition, the interaction results an enthalpy change (ΔH^o) of −0.201 ± 0.001 kcal/mol, a contribution from entropy ($T\Delta S^o$) of 8.103 ± 0.003 kcal/mol and a free energy change (ΔG^o) of −8.304 ± 0.005 kcal/mol. Contrarily, harmine-poly (rC).poly (rG) (Fig. 5B) calorimetric data with a stoichiometry of 6.916 nucleotide phosphates, produced a weak K_b value of $0.286 \pm 0.008 \times 10^6$ M^{-1}, an entropy change ($T\Delta S^o$) of 5.497 ± 0.001 kcal/mol and an enthalpy change (ΔH^o) of −1.946 ± 0.002 kcal/mol. Harmine binding with $tRNA^{phe}$ (Fig. 5C), showed a K_b $0.473 \pm 0.002 \times 10^6$ M^{-1}, (ΔH^o) of −0.331 ± 0.001 kcal/mol and $T\Delta S^o$ of 7.411 ± 0.004 kcal/mol. This interaction was seen to be similar to the previously explained Aristololactam-D-glucoside and Daunomycin binding to $tRNA^{phe}$ [108]. In addition, the strong positive entropy terms seen in the three cases where harmine was involved in interaction with the polynucleotides, point to the possibility of water molecules being disrupted and released, as well as partial-intercalative, stacking, and non-intercalative binding of the alkaloid into the corresponding nucleotide helix.

Moreover, using the standard relationship, $\Delta C_p^o = \partial(\Delta H)/\partial T$, the temperature dependence of the binding enthalpy determines the change in heat capacity (ΔC_p^o). For connecting structural and energetic data as well as for description of the hydration–dehydration that occur during the interaction, ΔC_p^o values are very significant. Calorimetric analysis was performed in 25–35 °C range and the

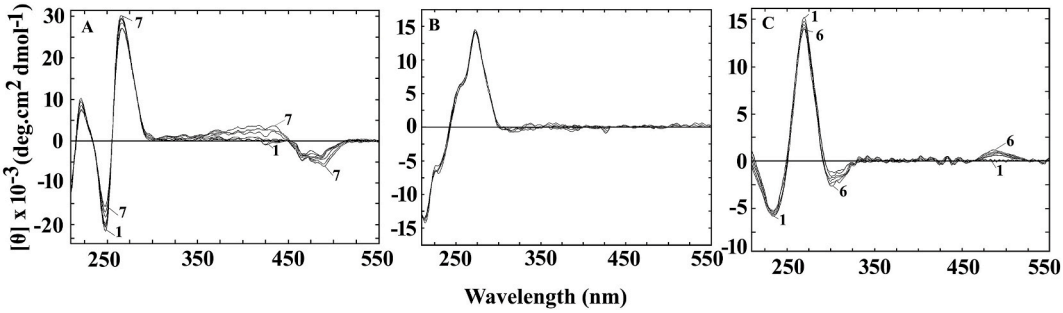

Fig. 4. Representative CD spectra resulting from interaction of (A) poly (rA) (65 μM) treated with 0, 30, 85, 120, 150, 180, 220 μM (curves 1–7) of harmine, (B) poly (rC)·poly (rG) (65 μM) treated with 0, 90, 120, 160, 200, 300 μM (curves 1–7) of harmine and (C) t-RNAphe (65 μM) treated with 0, 60, 90, 120, 180, 240 μM (curves 1–6) of harmine.

Table 2
Temperature-dependent thermodynamic parameters for the binding of harmine to poly (rA), poly (rC)·poly (rG) and t-RNA$^{ph.e}$.

RNA Polymers	Temperature (K)	K_b ($\times 10^6$ M^{-1})	N	ΔG^o /kcal mol^{-1}	ΔH^o /kcal mol^{-1}	$T\Delta S^o$ /kcal mol^{-1}
poly(A)	298.15	1.22 ± 0.04	4.080	−8.304 ± 0.005	−0.201 ± 0.001	8.103 ± 0.003
	303.15	0.824 ± 0.006	4.872	−8.207 ± 0.007	−0.505 ± 0.003	7.703 ± 0.007
	308.15	0.313 ± 0.004	4.887	−7.740 ± 0.008	−0.942 ± 0.001	6.800 ± 0.004
poly (rC)·poly (rG)	298.15	0.286 ± 0.008	6.916	−7.445 ± 0.006	−1.946 ± 0.002	5.497 ± 0.001
	303.15	0.191 ± 0.007	6.603	−7.325 ± 0.008	−4.395 ± 0.008	2.930 ± 0.009
	308.15	0.110 ± 0.005	6.600	−7.115 ± 0.009	−6.232 ± 0.007	0.883 ± 0.005
t-RNA^{phe}	298.15	0.473 ± 0.002	6.450	−7.742 ± 0.009	−0.331 ± 0.001	7.411 ± 0.004
	303.15	0.193 ± 0.008	6.633	−7.332 ± 0.008	−0.975 ± 0.002	6.357 ± 0.008
	308.15	0.121 ± 0.002	6.444	−7.164 ± 0.004	−1.451 ± 0.001	5.713 ± 0.003

[a]All the data in this table are derived from ITC experiments conducted in the same buffer, pH 6.8 and are average of three determinations. K_b and ΔH^o values were determined from ITC profiles fitting to Origin 7 software as described in the text. The values of ΔG^o and $T\Delta S^o$ were determined using the equations $\Delta G^o = -RT \ln K_b$ and $T\Delta S^o = \Delta H^o - \Delta G^o$.

thermodynamic parameters elucidated are collated in Table 2. Figs. S4 and S5 showed the ITC profile for titration of the polynucleotides (1000 μM) into 10 μM harmine solution at 30 °C and 35 °C, respectively. The association constant for harmine binding to poly (rA) varied from $1.22 \pm 0.01 \times 10^6$ M^{-1} at 25 °C to $0.313 \pm 0.004 \times 10^6$ M^{-1} at 35 °C. It was entropy driven interactions at all the three temperatures. Subsequently, the Gibbs energy exhibited only small changes (varied from −8.304 ± 0.005 to −7.740 ± 0.008 kcal/mol). The enthalpy changes at different temperatures produced heat capacity ΔC_p^o estimation. A value of −0.137 kcal/mol K was determined from slope of the line. On the other hand, the binding constant of the complexation for harmine with tRNA^{phe} varied from $0.473 \pm 0.002 \times 10^6$ M^{-1} at 25 °C to $0.121 \pm 0.002 \times 10^6$ M^{-1} at 35 °C. This interaction exhibited small changes in Gibbs energy that varied from −7.742 ± 0.009 to −7.164 ± 0.004 kcal/mol. The binding enthalpy increased and the entropy term (a favorable term to the Gibbs energy) decreased with increase in temperature keeping ΔG^o almost constant. A value of −0.112 kcal/mol K was obtained from the heat capacity (ΔC_p^o) (Fig. 6A–B). The Gibbs energy is compensated by the reaction entropy and enthalpy, both of which are significant temperature-dependent factors. Many ligands' interactions with RNA [48,49] as well as with DNA [104–107] have been reported to include this type of compensation. It is proposed that the phenomena are caused by a significant hydrophobic component to the binding energies. Small negative ΔC_p^o values are associated with a minimal sequence specific binding [109]. By extending the argument, it can be said that the slightly negative non-zero ΔC_p^o value that is shown here for harmine binding to the aforementioned RNA polynucleotide complexation, indicates binding that is structure specific.

Furthermore, from the relationship, $\Delta G_{hyd} = 80\ (\pm 10) \times \Delta C_p^o$, the Gibbs energy contribution from the hydrophobic transfer of binding with harmine may be analyzed [110]. The range of ΔG_{hyd} that is observed for intercalating compounds is reported to be between −10/kcal mol−1 and −14/kcal mol−1 [111]. Hence, from the obtained ΔG_{hyd} values of −10.96/kcal mol^{-1} and −8.96/kcal mol^{-1} for poly (rA) and tRNA^{phe}, respectively, it may be expected to be intercalative and partial intercalative interactions (Fig. 6A and B). This assumption regarding mode of binding of harmine also supports the analysis by ferrocyanide quenching (*vide supra*).

Based on the above spectroscopic and calorimetric assays harmine shows non-isosbestic UV spectroscopic interaction with enhancement of fluorescence intensity with the above RNA motifs. The interaction further showed exothermic and entropy-driven binding. From mode of binding and stability point of view, harmine adopts a partial intercalative binding with poly (rA) and tRNA^{phe}, and stronger binding free energy was observed with poly (rA). In contrast, the stacking forces with poly (rC)·poly (rG) were comparatively less pronounced and adopts a groove binding mode. However, with double stranded CT-DNA as reported by the authors, harmine showed isosbestic UV spectroscopic interaction with cooperative mode of binding, almost 85 % quenching in fluorescence intensity and the interaction showed partial intercalative, exothermic and entropy-driven binding [36].

3.7. Molecular docking

Further, to assess the binding profile of harnime (HRM) with the polynucleotide sequences *viz.*, poly (rA) (PA), poly (rC). poly (rG) (PGC), and tRNA^{phe} (TRNA), a comprehensive set of in-silico techniques were employed, involving molecular docking, dynamics simulations and MM/PBSA calculations.

Initially, molecular docking studies were conducted on the polynucleotide-ligand systems, allowing HRM to freely explore the entire length of the polynucleotide sequences. This approach facilitated the assessment of the binding mode and binding affinity of HRM with each polynucleotide sequence. The results revealed that HRM binds to the upper central region of both polynucleotide sequences, PA and PGC, demonstrating partial intercalative and groove binding, respectively, with both the sequences. The average binding affinities of HRM with PA and PGC were found to be −5.8 kcal/mol and −3.6 kcal/mol, respectively. Notably, in these complexes, hydrophobic interactions between the aromatic rings of HRM and the base pairs, as well as hydrogen bonds formed between the –NH and –OH groups of HRM and the surrounding base pairs, that played significant roles in the stabilization of the complex. In case of TRNA, HRM was found to bind specifically in the TΨC arm of the acceptor domain, with an average binding affinity of −4.5 kcal/mol. In this complex, pi-pi stacked interactions were observed between the three aromatic rings of HRM and the target, while the methyl groups formed pi-alkyl interactions with the adjacent base pairs. Furthermore, hydrogen bonds were also formed between the –NH and –OH groups of HRM and the binding site base pair. From the docking results, the docked poses exhibiting the highest binding

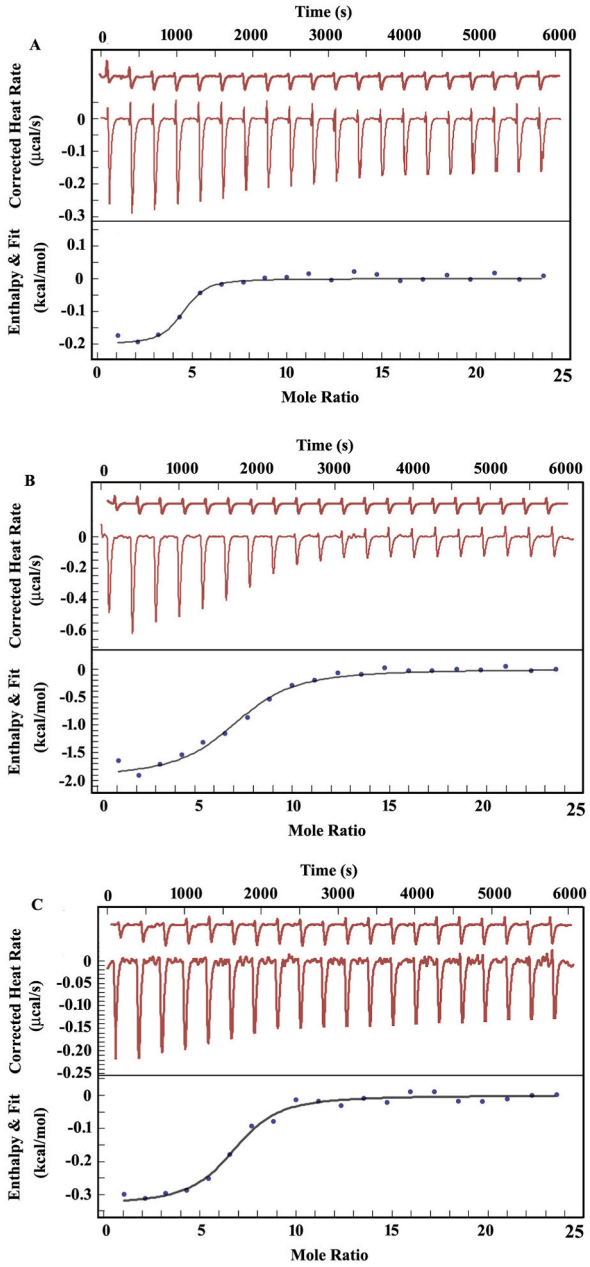

Fig. 5. Representative ITC profile for titration of 1000 μM each of (A) poly (rA), (B) poly (rC)·poly (rG) and (C) t-RNAphe into 10 μM harmine solution at 25 °C. Each heat burst curve (upper panel) represents the outcome of a 10 μL injection of the polynucleotides into the ligand solution. The bottom section shows the normalized heat signals vs molar ratio. The data points (●) indicate the experimental injection heat, while the solid line represents the estimated data fit.

affinity for each target were selected for subsequent molecular dynamics (MD) simulations.

3.8. Molecular dynamics

Valuable insights were gained into the multi-RNA binding profile of HRM with PA, PGC and TRNA through the analysis of the molecular dynamic simulations of the complexes. These simulations allowed for the exploration of the stability of the drug-polynucleotide complexes in a dynamic solvent system, shedding light on the dynamic nature of the interactions involved in complex formation. This approach provided a deeper understanding of the significant interactions driving the binding of HRM with the above polynucleotide sequences.

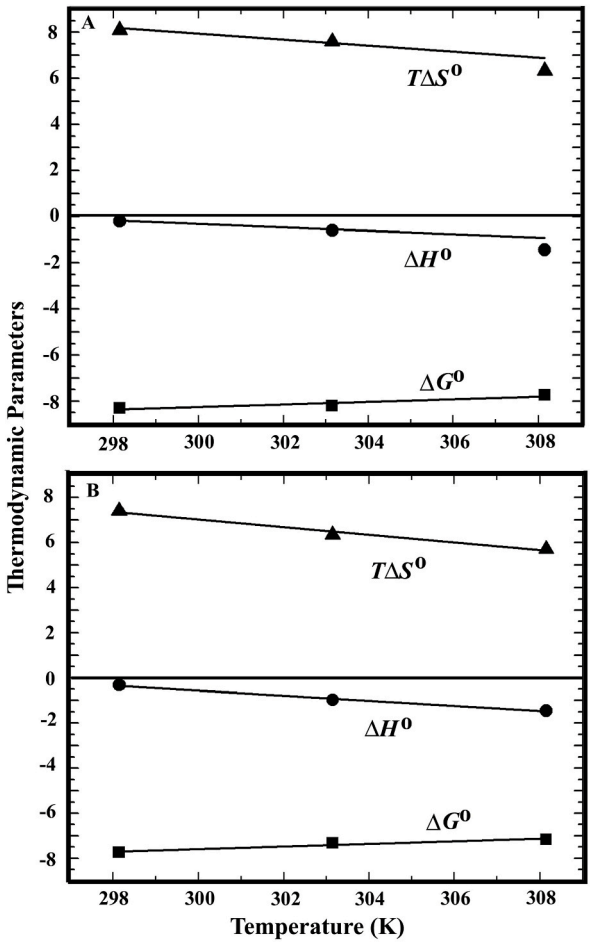

Fig. 6. Temperature dependent thermodynamic parameters, $T\Delta S^\circ$, ΔH°, and ΔG° for (A) poly (rA), (B) $tRNA^{phe}$ binding to harmine. Values of all the parameters are presented in the text.

3.8.1. HRM binding: insights into PA, PGC and TRNA interactions

Root Mean Square Deviations (RMSD) were calculated to ascertain the stability of the complexation in a dynamic solvent environment. The RMSD plots of the polynucleotide sequences PA and PGC (Fig. 7A and B), portray higher fluctuations which can be attributed to the terminal base pair fraying associated with the structure of the polynucleotide sequences. The occurrence of terminal base pair fraying is a widely observed phenomenon in MD simulations of nucleotide sequences, particularly when the terminal base pairs consist of Adenine and Thymine [112]. Interestingly, on binding of HRM to the polynucleotide sequences, the fluctuations are stabilized due to the additional base stacking provided by the presence of HRM which reduces the base pair fraying and increases the structural steadiness of the polynucleotide sequences and thereby establishes complex stability. Furthermore, the single-stranded structure of PA showed bending at the interacting site, indicating a possible transition from the single strand to double strand due to the binding of HRM. The structural similarities of the receptors and stability were monitored by calculating the eRMSD values, which are below 1.5 Å for all the three receptors. The values indicate that deviation of structural conformation of the receptor is not major, and the structure remains stable throughout the simulations. To further assess the result of HRM binding on the overall structural compactness of the polynucleotide sequences, Radius of Gyration (Rg) was calculated and analyzed (Fig. 7C and D). The results of Rg suggest that HRM induces a marginal increase in the flexibility on the overall structure of both the polynucleotide sequences. Upon visualizing the trajectory of the HRM-PA complex, we further observed that HRM engages in base stacking with the PA nucleobases. This interaction promotes stable complexation and reduces base pair fraying compared to PA in the absence of the ligand. These stacking forces played a crucial role in stabilizing the complex formation between HRM and PA. To analyze the degree of base stacking between HRM and the binding site residues, representative MD poses were extracted after 40 ns, when the complex achieves stability (Fig. 8A). HRM was found to bind in the central region of the single strand, specifically between the nucleobases Adenine 4 and 5. At 44 ns, HRM aligned itself with Adenine 5 and formed pi-pi stacked interactions with its purine ring system. The resulting base stacking forces with Adenine 5 were consistently maintained by the ligand throughout the trajectory, serving as a major contributor to the steadiness of the formation of complex. Between 70 and 80 ns, a notable shift occurred as the nucleobase Adenine 4 moved above HRM, with its purine ring positioned perpendicular to the drug. This new orientation led to weaker pi-alkyl interactions between

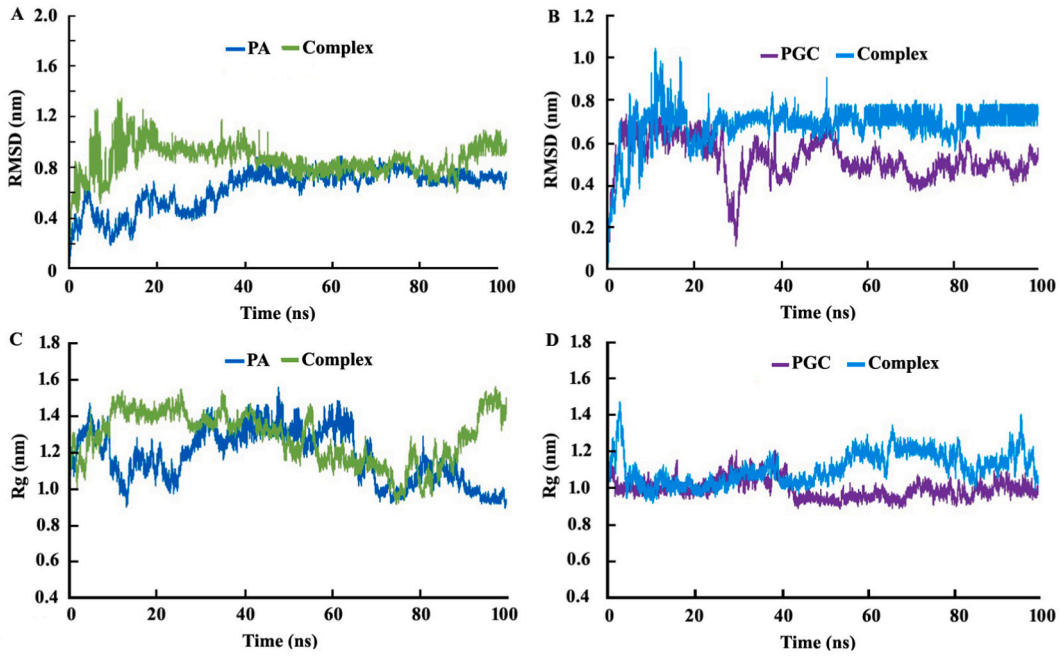

Fig. 7. RMSD of HRM with (A) PA and (B) PGC, Rg of HRM with (C) PA and (D) PGC.

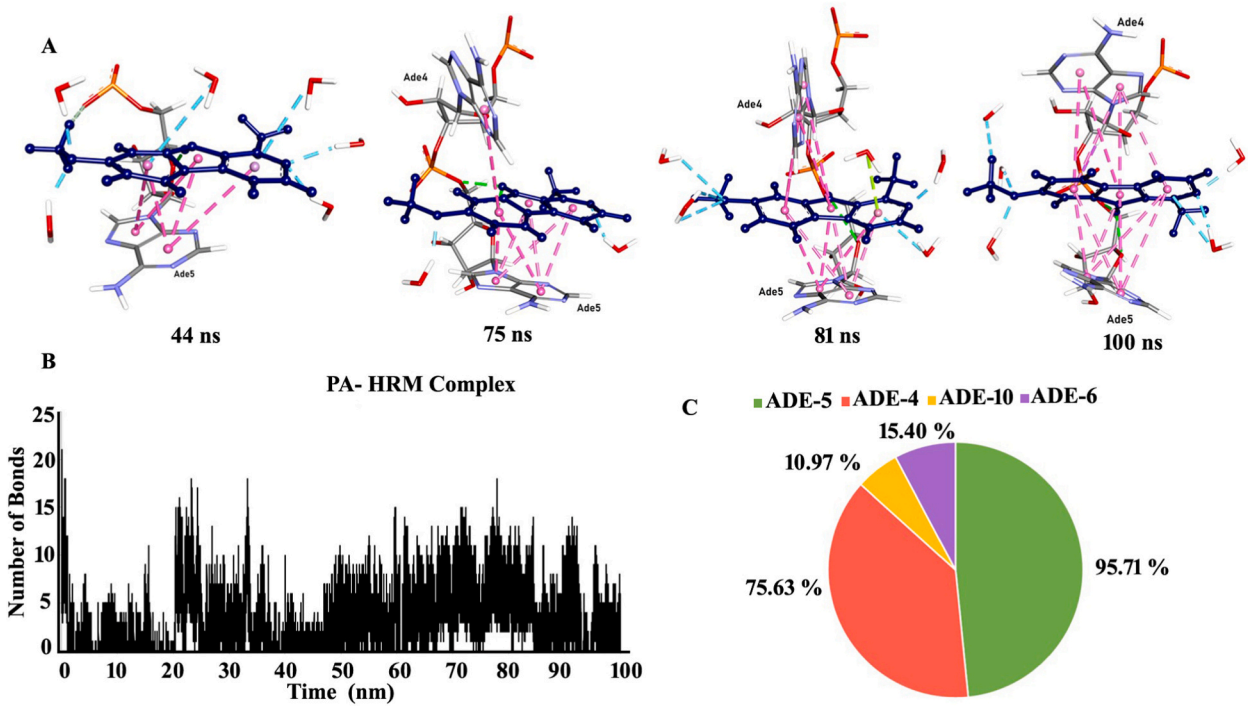

Fig. 8. (A) Representative MD poses of HRM-PA complex and their binding interactions in 3D representation, (B) Number of Bonds representation and (C) Occupancy of the stable binding interactions.

Adenine 4 and HRM. Furthermore, the shift brought the backbone closer to the ligand, allowing the –NH group of HRM to form hydrogen bonds with the backbone and sugar molecules of both nucleobases. Adenine 4 underwent further changes in orientation and eventually settled into a parallel position above HRM. In this configuration, the drug establishes enhanced pi-pi stacked interactions with both nucleobases, resulting in a partial intercalation binding with the PA polynucleotide sequence. These partial intercalation

patterns observed in the computational results aligned with the experimental findings. Although it is imperative to acknowledge the inherent limitations in capturing complete thermodynamic convergence for flexible chains like Poly-A within the relatively short timescales of MD simulations. The study's duration is indeed restricted, and it is essential to recognize that molecular relaxation processes, which can span micro-milliseconds, remain beyond the scope of our investigation. The conformational changes observed in Poly-A through experimental measurements may not be entirely captured within the confines of our brief MD simulations. The occupancy rate of the binding interactions analyzed shows that the stacking forces with the Adenine 5 were present for 96 % of the trajectory while that with Adenine 4 were present for 75 % establishing a partial intercalation with the polynucleotide sequence and stabilized the complex formation of HRM with PA (Fig. 8 B, C). Furthermore, the equilibrated conformation of PA after binding with harmine has been depicted in Fig. S6 (a1 and b1).

In the case of HRM binding with PGC, the stacking forces were observed to be less pronounced compared to the HRM-PA complexation. HRM was found to bind between Guanine 5 and Cystine 6, with only Guanine 5 exhibiting a favorable base stacking alignment (Fig. 9A). The aromatic rings of HRM form pi-pi stacked interactions with the purine ring of the nucleobase, while the –N atom of the ring establishes a hydrogen bond with the sugar molecule of Guanine 5. Fig. S6 (a2 and b2) shows the equilibrated structure of PGC after binding with harmine.

Additionally, the other –NH and –OH groups of HRM form hydrogen bonds with water molecules in the surrounding environment (Fig. 9 B). RMSD graphs comparing TRNA in the presence and absence of HRM indicate that HRM binds to TRNA with minimal fluctuations (Fig. 10 A). These fluctuations may be attributed to the fraying of base pairs and subtle conformational changes of the bases within the domains, influenced by the dynamic solvent environment. The Rg plots shows that, for the majority of the simulation, the structural compactness of TRNA is slightly reduced, accompanied by a marginal increase in nucleobase flexibility (Fig. 10 B). Interestingly, after 60 ns, the structural compactness of TRNA starts to increase, indicating a rigidification of the nucleobases. This rigidification may be attributed to enhanced interactions that stabilize the complex formation between HRM and TRNA. The binding of HRM to TRNA was primarily stabilized by hydrophobic interactions showing a partial intercalation binding with TRNA. The aromatic rings of HRM engaged in pi-pi stacked and pi-alkyl interactions with the purine and pyrimidine rings of the nucleobases at the binding site (Fig. 10C). Additionally, the –OH group of HRM formed hydrogen bonds with the nucleobases (Fig. 10 D). These increased interactions between HRM and the nucleobases restricted their conformational degree of freedom and contributed to the enhanced structural compactness observed in the Rg results. Fig. S6 (a3 and b3) shows the structure of TRNA alone and equilibrated structure of TRNA after binding with harmine.

3.8.2. Principal Component Analysis (PCA)

To gain a comprehensive understanding of the intricate structural changes induced by the binding of harmine on the selected RNA structures, Principal Component Analysis (PCA) was conducted on the nucleobases. PCA emerges as an invaluable analytical approach, facilitating the visualization of synchronized atomic displacements within macromolecules during molecular dynamics (MD) trajectories [85,86,113–117]. Remarkably, the initial three Eigen vectors collectively accounted for approximately 50–80 % of the dynamic motions. The juxtaposition of major principal components on a 2D plane offers a clear depiction of atomic displacement patterns (Figs. 11–13) [85,86,113]. PC1, PC2, and PC3 were plotted against one another to visually assess the structural disparities that may have induced during the binding of harmine to the above structures. The relative eigenvalues, which signify the percentage of total mean square displacement (or variance) of atom-position fluctuations.

Obtained PCA results suggest that PA shows stable structural variations caused by the partial intercalation of harmine and terminal base pair fraying as indicated by the congregation of majority of the data points in the central portion of the PCA plot (Fig. 11a, c). Minimum fluctuations were observed in the binding site area suggesting that the intercalation supported by the strong stacking forces restricts the movement of the nucleobases and stabilizes the complex formation (Fig. 11 b). Conversely, substantial fluctuations were

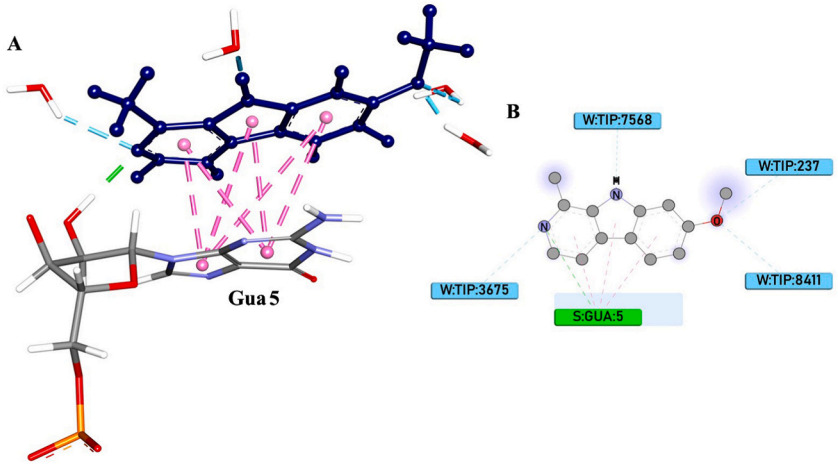

Fig. 9. Binding interactions of HRM with PGC (A) 3D representation and (B) 2D representation.

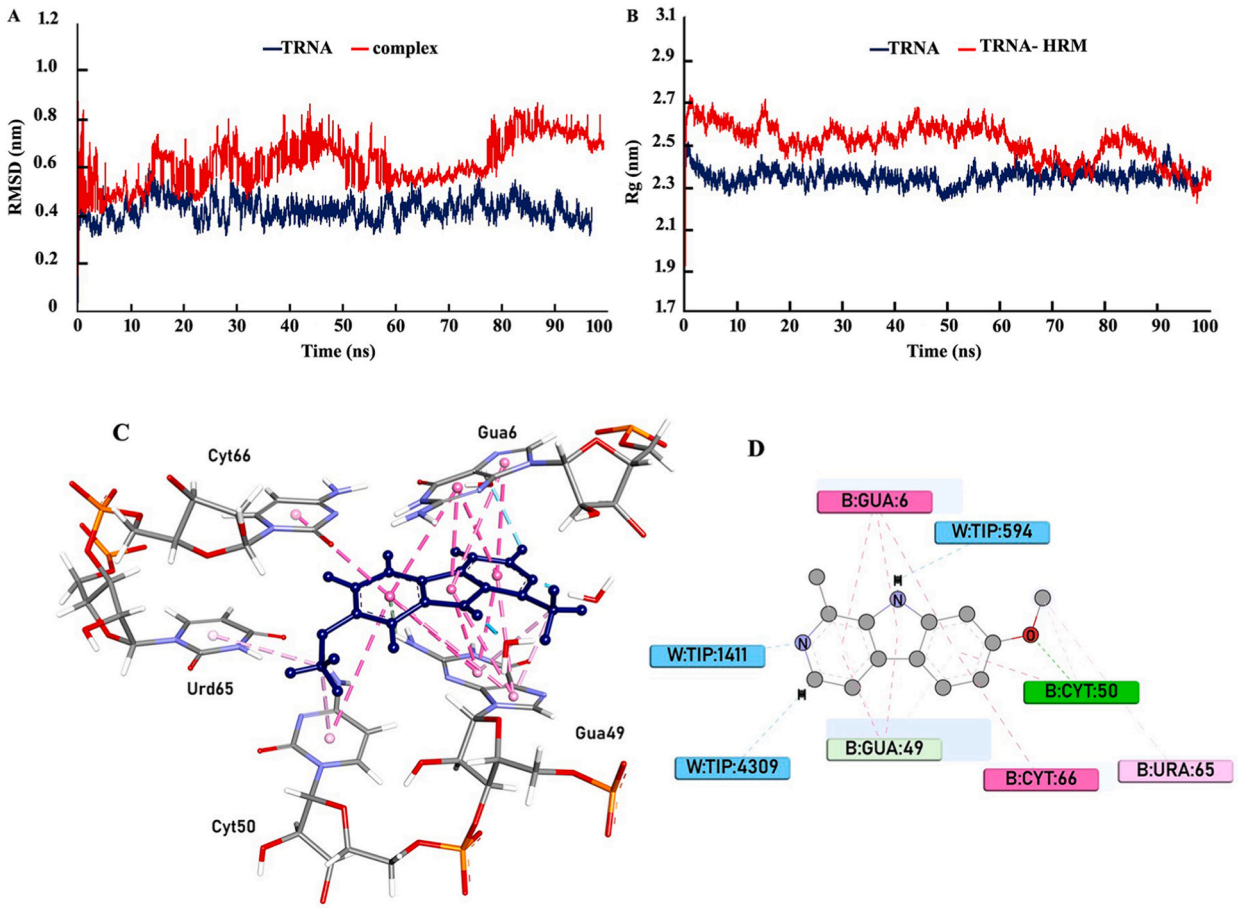

Fig. 10. TRNA with HRM complex formation (A) RMSD and (B) Rg representation. Binding interactions of HRM with TRNA (C) 3D representation and (D) 2D representation. Encapsulated within each dimension, were also computed, and presented. The color gradient – transitioning from blue to white to red – indicates the recurring shifts among conformers throughout the trajectory.

observed in the terminal nucleobases, indicating heightened mobility in these regions (Fig. 11 b). This phenomenon aligns with the single-strand to double-strand transition observed in PA, as substantiated by both experimental evidence and the visualization of MD simulations.

Similar terminal base pair fraying was also observed in the structure of PGC with maximum fluctuations observed in PCA RMSF plot (Fig. 12 a-c) while the binding site nucleobases reflected only minimum fluctuations suggesting that binding with harmine restricts the movement of nucleobases by forming stable interactions in minor groove of the nucleic acid.

The structural variations observed in TRNA are slightly more prominent with the data points clustered in an elliptical form suggesting that TRNA has a greater conformational range as compared to the other two RNA receptors (Fig. 13 a). Interestingly, as indicated by the PCA RMSF plot, the maximum fluctuations are observed in the terminal and elbow regions of TRNA, far from the binding site (Fig. 13 b, c). Conversely, the binding site domain portrays minimum fluctuations which can be attributed to the stable stacking forces provided by the binding of harmine. Validation of the structural variations within each nucleotide is further substantiated by representative MD poses extracted across the 100 ns simulations, coupled with experimental data. Through this methodical investigation, we gain substantial insights into the evolving structural landscape and dynamics of the polynucleotides on binding with the ligand.

3.8.3. Energy evaluations: MM/PBSA

The stable trajectories of HRM complexes with PA, PGC and TRNA were analyzed for their respective binding free energies through MM/PBSA calculations. The results of the individual energetic terms including the entropic component are provided in Table 3. The results indicate that HRM binding with TRNA and PA are more energetically favorable than with PGC.

4. Conclusion

Apart from the above conformations of RNA, there are many other RNA motifs, and drugs that are meant to bind to specific

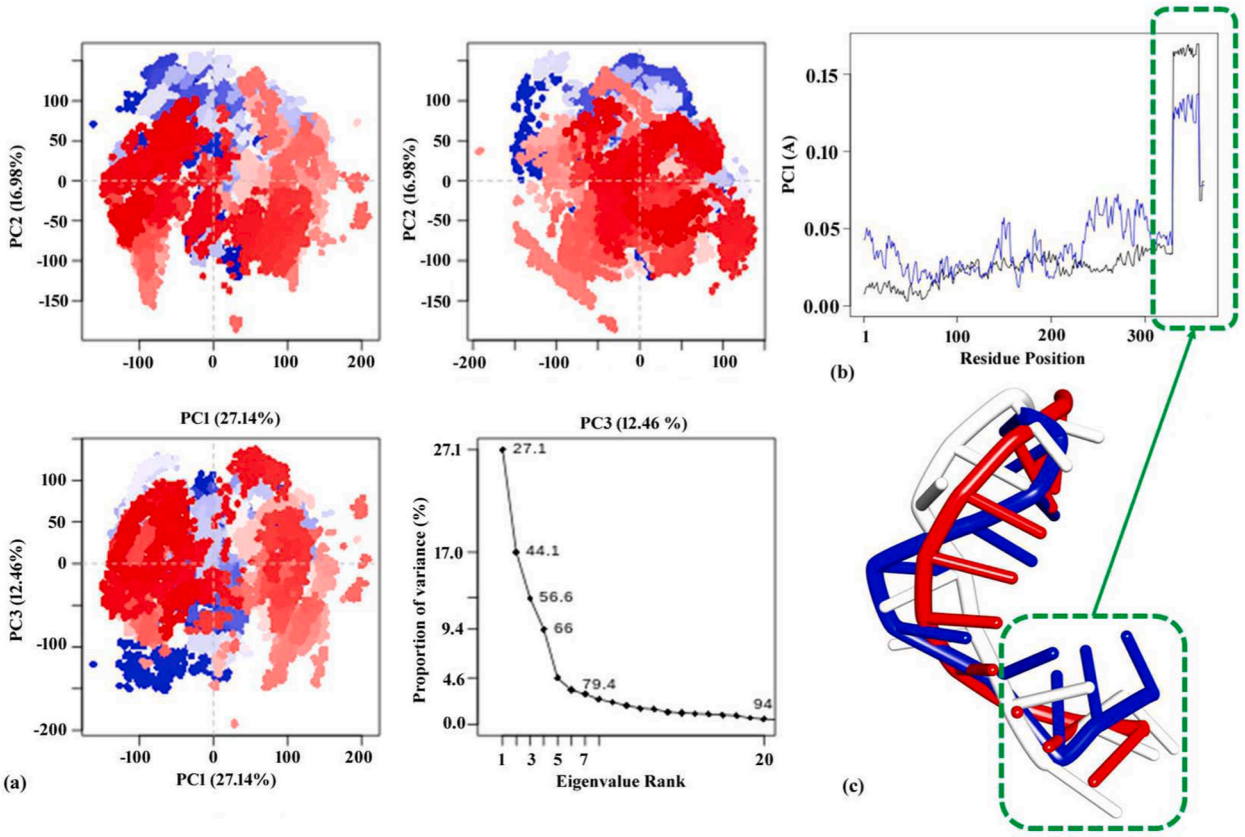

Fig. 11. (a) PCA cluster plot and Scree plot, (b) PCA RMSF plot, (c) Superimposed MD poses of PA extracted at 0 ns (red), 50 ns (white) and 100 ns (blue).

sequences or structural patterns. Hence this study of harmine binding to the above three RNAs has no immediate application but rather serves as a future promising biochemical and biophysical characterization of RNA-small molecule interactions.

From the standpoint of designing of potential RNA targeted drugs, and the diverse conformational variations found in the RNA structures, our data here present significant insights into the nature of binding of the small molecule. Throughout this investigation based on spectroscopic, calorimetric and molecular docking and dynamics, binding of the alkaloid, harmine depends on the suitability to the geometry of the RNA nucleotides that showed maximum preference with single stranded poly (rA) followed by moderate binding with clover leaf structure of $tRNA^{phe}$ and least with homopolymer of A-form double stranded structure of poly (rC).poly (rG).

Harmine is presumed to induce single stranded to double stranded conformational change in poly (rA). Many small molecules have been reported to induce such single stranded to double stranded conformational change in poly (rA), called self-structure induction, at physiological pH [26,54,55,118–121]. This was assumed to be an antiparallel duplex formation in poly (rA). The self-structure of polyribonucleic acid A by harmine has been assumed in this research based on the results of differential scanning calorimetry and a cooperative UV absorbance melting profile. (Fig. S7). The melting profile generated by differential scanning calorimetry showed a two-state transition with a ratio of the calorimetric and van't Hoff enthalpy close to unity for the melting of the self-structure of harmine-induced poly (rA) complex. Self-structure formation in single-stranded poly (rA) is a potential strategy that can switch off protein synthesis and bring a novel approach for the improvement of RNA-based therapeutic agents against cancer like disorder. While with rigid clover leaf motif in $tRNA^{phe}$ structure, harmine showed moderate binding at the TΨC arm. On the other hand, steric hindrance by the 2-NH_2 group of guanine in the homopolymer of A-form poly (rC).poly (rG) is significant enough to make the structure more shallow, wide, and electrostatically positive and due to features such as the 2′-OH group in the RNA minor groove [46], provide least acceptability compared to the other aforesaid polynucleotide structures for harmine to bind. Comparing the binding site and binding location of harmine inside the aforesaid varied RNA polynucleotide motifs, the findings from the molecular dynamics simulations further shed light on the binding behavior of harmine with the polynucleotides. It was observed that harmine adopts a partial intercalative binding mode with both poly (rA) and $tRNA^{phe}$. This binding mode is characterized by pronounced stacking forces and a stronger binding free energy observed specifically with poly (rA) followed by $tRNA^{phe}$. Interestingly, the stacking forces between harmine and poly (rC).poly (rG) were relatively less pronounced, making intercalative binding less favorable and showed groove binding more probable. The association between harmine and poly (rA) led to notable changes in the structural configuration, primarily influenced by the partial intercalative mode of binding adopted by the drug. This transformation is discernible through the

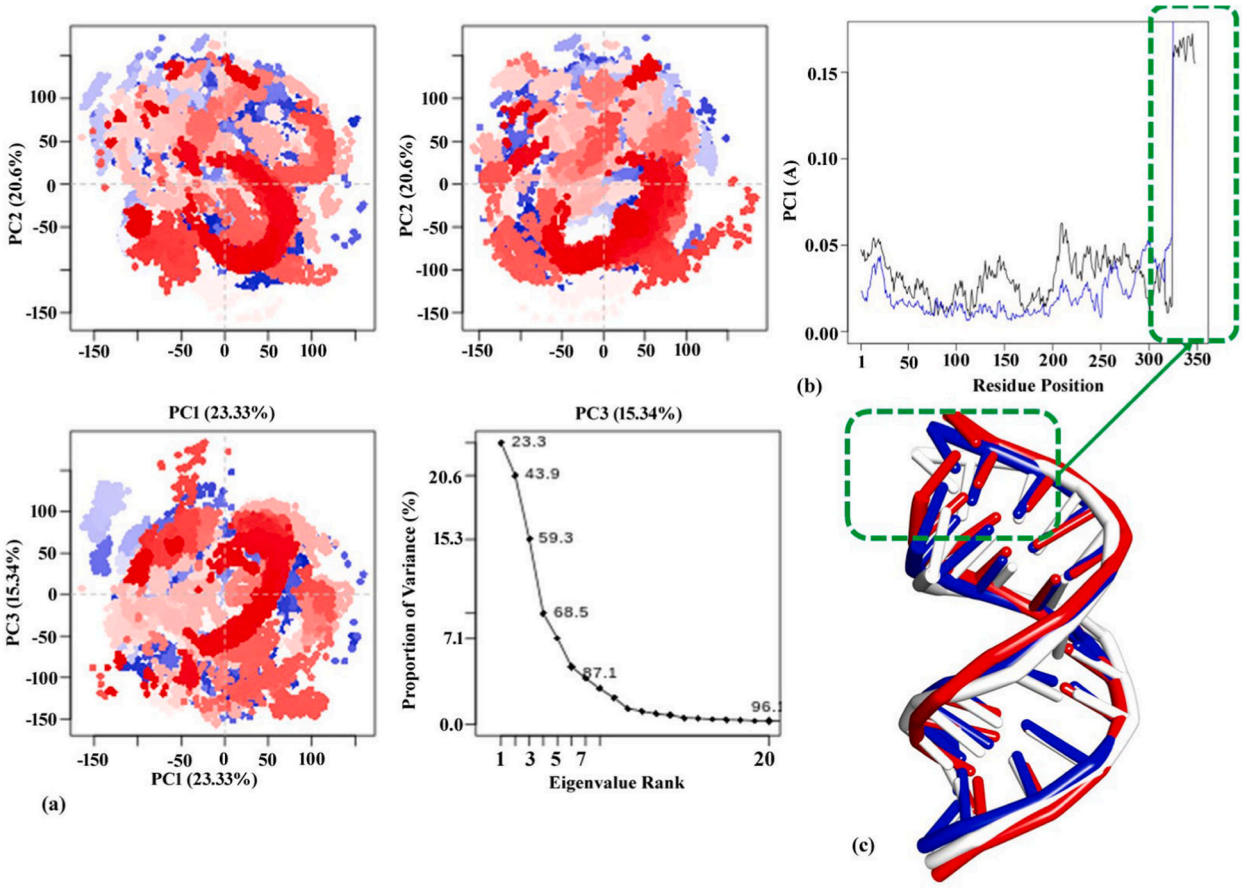

Fig. 12. (a) PCA cluster plot and Scree plot, (b) PCA RMSF plot, (c) Superimposed MD poses of PGC extracted at 0 ns (red), 50 ns (white) and 100 ns (blue).

heightened RMSD graph (Fig. S8), and is further elucidated by the analyses of Rg and PCA, which collectively capture the nuanced shifts and dynamics within the poly (rA) structure induced by harmine binding. These observations indicated that the binding characteristics of harmine vary, depending on RNAs of different motifs and showed a clear specificity towards the single stranded poly (rA) compared to the other motifs. Thus, these results further advance our fundamental understanding towards small molecule-RNA interaction.

Data availability statement

Data will be made available on request.

CRediT authorship contribution statement

Paromita Sarkar: Software, Methodology, Investigation, Formal analysis, Data curation. **Priyanka Gopi:** Software, Investigation, Formal analysis, Data curation. **Prateek Pandya:** Validation, Software, Methodology, Investigation, Formal analysis, Data curation. **Samaresh Paria:** Methodology, Formal analysis, Data curation. **Maidul Hossain:** Validation, Software, Methodology, Investigation, Formal analysis, Data curation. **Manzer H. Siddiqui:** Software, Investigation, Funding acquisition. **Saud Alamri:** Software, Investigation, Funding acquisition. **Kakali Bhadra:** Writing – review & editing, Writing – original draft, Visualization, Validation, Supervision, Resources, Project administration, Methodology, Investigation, Funding acquisition, Formal analysis, Data curation, Conceptualization.

Declaration of competing interest

The authors declare that they have no known competing financial interests or personal relationships that could have appeared to influence the work reported in this paper.

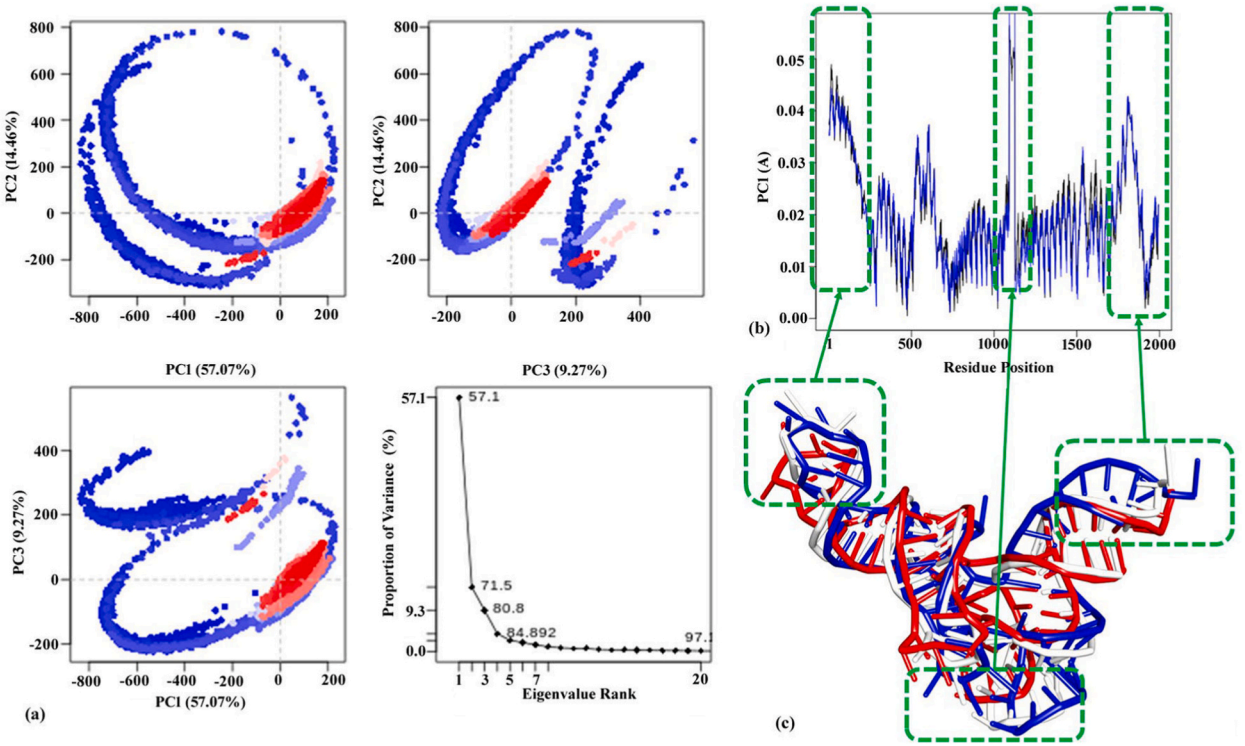

Fig. 13. (a) PCA cluster plot and Scree plot, (b) PCA RMSF plot, (c) Superimposed MD poses of TRNA extracted at 0 ns (red), 50 ns (white) and 100 ns (blue).

Table 3
Binding free energy changes with energy contributions of harmine with TRNA tRNA, PGC poly(C)·poly(G) and PA poly(A).

	PA	PGC	TRNA
$\Delta E_{VDWAALS}$	−19.7 ± 0.4	−16.81 ± 0.39	−29.65 ± 0.62
ΔE_{EL}	−22.36 ± 1.19	−5.91 ± 1.35	−37.28 ± 0.55
ΔE_{GB}	32.88 ± 0.92	14.43 ± 1.30	55.42 ± 0.64
ΔE_{SURF}	−1.41 ± 0.02	−1.16 ± 0.02	−1.98 ± 0.02
ΔG_{GAS}	−42.05 ± 1.38	−22.72 ± 1.51	−66.93 ± 0.63
ΔG_{SOLV}	31.47 ± 0.92	13.3 ± 1.3	53.43 ± 0.64
ΔTOTAL	−10.58 ± 0.56	−9.45 ± 0.37	−13.49 ± 0.48
Entropy	−0.57 ± 0.09	2.29 ± 0.48	1.37 ± 0.04
Δ*G* binding	**−11.15±1.37**	**−7.16±1.70**	**−12.12±1.17**

Acknowledgement

PS is indebted to URS, fellowship from UGC, Govt. Of India. The authors sincerely acknowledge the Researchers Supporting Project number (RSP2024R194), King Saud University, Riyadh, Saudi Arabia. DST-PURSE, PRG University of Kalyani, 2024-25 and DST-FIST SR/FST/LSI-467/2010C are recognized for the partial funding. Dr. Tapas Majumder, Department of Chemistry, University of Kalyani, to be acknowledged for providing the facility of fluorescence spectroscopy.

Appendix A. Supplementary data

Supplementary data to this article can be found online at https://doi.org/10.1016/j.heliyon.2024.e34183.

References

[1] Y. Zhu, L. Zhu, X. Wang, H. Jin, RNA-based therapeutics: an overview and prospectus, Cell Death Dis. 13 (2022) 644, https://doi.org/10.1038/s41419-022-05075-2.

[2] Y.-K. Kim, RNA therapy: rich history, various applications and unlimited future prospects, Exp. Mol. Med. 54 (2022) 455–465, https://doi.org/10.1038/s12276-022-00757-5.

[3] B. Chhatriya, M. Mukherjee, S. Ray, P. Sarkar, S. Chatterjee, D. Nath, K. Das, S. Goswami, Comparison of tumour and serum specific microRNA changes dissecting their role in pancreatic ductal adenocarcinoma: a meta-analysis, BMC Cancer 19 (2019) 1175, https://doi.org/10.1186/s12885-019-6380-z.

[4] B. Saha, B. Chhatriya, S. Pramanick, S. Goswami, Bioinformatic analysis and integration of transcriptome and proteome results identify key coding and noncoding genes predicting malignancy in intraductal papillary mucinous neoplasms of the pancreas, BioMed Res. Int. 2021 (2021) 1056622, https://doi.org/10.1155/2021/1056622.

[5] M. Mukherjee, S. Goswami, Identification of key deregulated RNA binding proteins in pancreatic cancer by meta-analysis and prediction of their role as modulators of Oncogenesis, Front. Cell Dev. Biol. 9 (2021) 713852, https://doi.org/10.3389/fcell.2021.713852.

[6] M. Mukherjee, S. Pramanik, B. Saha, B. Chhatriya, S. Goswami, Noncoding RNAs as key modulators of autophagy in pancreatic cancer (Review), Oncol, Report 46 (2021) 128–140, https://doi.org/10.3892/or.2021.8079.

[7] J. Gallego, G. Varani, Targeting RNA with small molecule drugs: therapeutic promise and chemical challenges, Acc. Chem. Res. 34 (10) (2001) 836–843, https://doi.org/10.1021/ar000118k.

[8] N. Foloppe, N. Matassova, F. Aboul-ela, Towards the discovery of drug-like RNA ligands, Drug Discov. Today 11 (21–22) (2006) 1019–1027, https://doi.org/10.1016/j.drudis.2006.09.001.

[9] S. Fulle, H. Gohlke, Molecular recognition of RNA: challenges for modeling interactions and plasticity, J. Mol. Recogn. 23 (2) (2010) 220–231, https://doi.org/10.1002/jmr.1000.

[10] W. Hong, J. Zeng, J. Xie, Antibiotic drugs targeting bacterial RNAs, Acta Pharm. Sin. B 4 (4) (2014) 258–265, 10.1016%2Fj.apsb.2014.06.012.

[11] D.P. Bartel, MicroRNAs: genomics, biogenesis, mechanism, and function, Cell 116 (2) (2004) 281–297, https://doi.org/10.1016/s0092-8674(04)00045-5.

[12] C.C. Esau, B.P. Monia, Therapeutic potential for microRNAs, Adv. Drug Deliv. Rev. 59 (2–3) (2007) 101–114, https://doi.org/10.1016/j.addr.2007.03.007.

[13] P. Nelson, M. Kiriakidou, A. Sharma, E. Maniataki, Z. Mourelatos, The microRNA world: small is mighty, Trends Biochem. Sci. 28 (10) (2003) 534–540, https://doi.org/10.1016/j.tibs.2003.08.005.

[14] L. Vukovic, H.R. Koh, S. Myong, K. Schulten, Substrate recognition and specificity of double-stranded RNA binding proteins, Biochemistry 53 (21) (2014) 3457–3466, https://doi.org/10.1021/bi500352s.

[15] K.-N. Son, Z. Liang, H.L. Lipton, Double-stranded RNA is detected by immune fluorescence analysis in RNA and DNA virus infections, including those by negative stranded RNA viruses, J. Virol. 89 (18) (2015) 9383–9392, https://doi.org/10.1128/jvi.01299-15.

[16] R. Srinivasan, U. Karaoz, M. Volegova, J. MacKichan, M. Kato-Maeda, S. Miller, R. Nadarajan, E.L. Brodie, S.V. Lynch, Use of 16S rRNA gene for identification of a broad range of clinically relevant bacterial pathogens, PLoS One 10 (2) (2015) e0117617, https://doi.org/10.1371/journal.pone.0117617.

[17] A. Son, S.I. Choi, G. Han, B.L. Seong, M1 RNA is important for the in-cell solubility of its cognate C5 protein: implications for RNA-mediated protein folding, RNA Biol. 12 (11) (2015) 1198–1208, https://doi.org/10.1080/15476286.2015.1096487.

[18] J. Guiro, S. Murphy, Regulation of expression of human RNA polymerase II-transcribed snRNA genes, Open Biol 7 (6) (2017) 170073, https://doi.org/10.1098/rsob.170073.

[19] S. Sarkar, P. Bhattacharjee, T. Ghosh, K. Bhadra, Pharmaceutical efficacy of harmalol in inhibiting hepatocellular carcinoma, Future J Pharmaceutical Sciences 6 (29) (2020) 1–18, https://doi.org/10.1186/s43094-020-00045-x.

[20] W. Saenger, in: C.R. Cantor (Ed.), Principles of Nucleic Acid Structure, Springer-Verlag, New York, 1983. New York.

[21] G.M. Blackburn, M.J. Gait, Nucleic Acids in Chemistry and Biology, IRL Press, Oxford University Press, 1990.

[22] M. Hossain, G.S. Kumar, DNA intercalation of methylene blue and quinacrine: new insights into base and sequence specificity from structural and thermodynamic studies with polynucleotides, Mol. Biosyst. 5 (2009) 1311–1322, https://doi.org/10.1039/B909563B.

[23] M. Hossain, G.S. Kumar, DNA binding of benzophenanthridine compounds sanguinarine versus ethidium: comparative binding and thermodynamic profile of intercalation, J. Chem. Thermodyn. 41 (6) (2009) 764–774, https://doi.org/10.1016/j.jct.2008.12.008.

[24] K. Bhadra, G.S. Kumar, Therapeutic potential of isoquinoline alkaloids: an update on their nucleic acids binding aspects and implications for drug design, Med. Res. Rev. 31 (6) (2011) 821–862, https://doi.org/10.1002/med.20202.

[25] R. Sinha, M. Hossain, G.S. Kumar, RNA targeting by DNA binding drugs: structural, conformational and energetic aspects of the binding of quinacrine and DAPI to A-form and HL-form of poly(rC)-poly(rG), Biochim. Biophys. Acta 1770 (2007) 1636–1650, https://doi.org/10.1016/j.bbagen.2007.08.018.

[26] P. Giri, G.S. Kumar, Self-structure induction in single stranded poly(A) by small molecules: studies on DNA intercalators, partial intercalators and groove binding molecules, Arch. Biochem. Biophys. 474 (2008) 183–192, https://doi.org/10.1016/j.abb.2008.03.013.

[27] M.M. Islam, S. Roy Chowdhury, G.S. Kumar, Spectroscopic and calorimetric studies on the binding of alkaloids berberine, palmatine and coralyne to double stranded RNA polynucleotides, J. Phys. Chem. B 113 (2009) 1210–1224, https://doi.org/10.1021/jp806597w.

[28] Z.P. Chen, J.B. Schell, C.-T. Ho, K.Y. Chen, Green tea epigallocatechin gallate shows a pronounced growth inhibitory effect on cancerous cells but not on their normal counterparts, Cancer Lett. 129 (2) (1998) 173–179, https://doi.org/10.1016/s0304-3835(98)00108-6.

[29] S.D. Sekaran, S.S. Leow, N. Abobaker, K.K. Tee, K. Sundram, R. Sambanthamurthi, M.B. Wahid, Effects of oil palm phenolics on tumor cells *in vitro* and *in vivo*, Afr. J. Food Sci. 4 (8) (2010) 495–502.

[30] P. Gao, N. Tao, Q. Ma, W.-X. Fan, C. Ni, H. Wang, Z.-H. Qin, DH332, a synthetic β-carboline alkaloid, inhibits B cell Lymphoma growth by activation of the caspase family, Asian Pac. J. Cancer Prev. APJCP 15 (9) (2014) 3901–3906, https://doi.org/10.7314/apjcp.2014.15.9.3901.

[31] M.H. Sehitoglu, A.A. Farooqi, M.Z. Qureshi, G. Butt, A. Aras, Anthocynins: targeting of signaling networks in cancer cells, Asian Pac. J. Cancer Prev. APJCP 15 (5) (2014) 2379–2381, https://doi.org/10.7314/apjcp.2014.15.5.2379.

[32] P.-M. Li, Y.-L. Li, B. Liu, W.-J. Wang, Y.-Z. Wang, Z. Li, Curcumin inhibits MHCC97H liver cancer cells by activating ROS/TLR-4/Caspase signaling pathway, Asian Pac. J. Cancer Prev. APJCP 15 (5) (2014) 2329–2334, https://doi.org/10.7314/apjcp.2014.15.5.2329.

[33] M. Greenwell, P.K.S.M. Rahman, Medicinal Plants: their use in anticancer treatment, Int. J. Pharma Sci. Res. 6 (10) (2015) 4103–4112, https://doi.org/10.13040/ijpsr.0975-8232.6(10).4103-12.

[34] J. Sharifi-Rad, A. Ozleyen, T.B. Tumer, C.O. Adetunji, N.I. Omari, A. Balahbib, Y. Taheri, A. Bouyahya, M. Martorell, N. Martins, W.C. Cho, Natural products and synthetic analogs as a source of antitumor drugs, Biomolecules 9 (11) (2019) 679, https://doi.org/10.3390/biom9110679.

[35] L. Liu, T. Zhao, X.M. Cheng, C.H. Wang, Z.T. Wang, Characterization and determination of trace alkaloids in seeds extracts from peganum harmala linn. Using LC–ESI–MS and HPLC, Acta Chromatogr. 25 (2) (2013) 221–240, https://doi.org/10.1556/AChrom.25.2013.2.2.

[36] S. Sarkar, P. Tribedi, K. Bhadra, Structure-activity insights of harmine targeting DNA, ROS inducing cytotoxicity with PARP mediated apoptosis against cervical cancer, anti-biofilm formation and *in vivo* therapeutic study, J. Biomol. Stuct. Dyn. 40 (2022) 5880–5902, https://doi.org/10.1080/07391102.2021.1874533.

[37] J.P. Taylor, L.H. Armitage, D.L. Aldridge, M.N. Cash, M.A. Wallet, Harmine enhances the activity of the HIV-1 latency-reversing agents ingenol A and SAHA, The Company of Biologists Ltd Biology Open 9 (2020) bio052969, https://doi.org/10.1242/bio.052969.

[38] R. Herrendorff, M.T. Faleschini, A. Stiefvater, B. Erne, T. Wiktorowicz, F. Kern, M. Hamburger, O. Potterat, J. Kinter, M. Sinnreich, Identification of plant-derived alkaloids with therapeutic potential for myotonic dystrophy type I, J. Biol. Chem. 291 (33) (2016) 17165–17177, https://doi.org/10.1074/jbc.M115.710616.

[39] Q. Chen, R. Chao, H. Chen, X. Hou, H. Yan, S. Zhou, W. Peng, A. Xu, Antitumor and neurotoxic effects of novel harmine derivatives and structure-activity relationship analysis, Int. J. Cancer 114 (5) (2005) 675–682, https://doi.org/10.1002/ijc.20703.

[40] J. Asgarpanah, F. Ramezanloo, Chemistry, pharmacology and medicinal properties of peganum harmala L, Afr. J. Pharm. Pharmacol. 6 (22) (2012) 1573–1580, https://doi.org/10.5897/AJPP11.876.

[41] F.A. Khan, A. Maalik, Z. Iqbal, I. Malik, Recent pharmacological developments in beta-carboline alkaloid “harmaline”, Eur. J. Pharmacol. 721 (1–3) (2013) 391–394, https://doi.org/10.1016/j.ejphar.2013.05.003.

[42] S. Nafisi, M. Bonsaii, P. Maali, M.A. Khalilzadeh, F. Manouchehri, β-Carboline alkaloids bind DNA, J. Photochem. Photobiol. B Biol. 100 (2) (2010) 84–91, https://doi.org/10.1016/j.jphotobiol.2010.05.005.

[43] S. Sarkar, K. Bhadra, Binding of alkaloid harmalol to DNA: photophysical and calorimetric approach, J. Photochem. Photobiol. B Biol. 130 (2014) 272–280, https://doi.org/10.1016/j.jphotobiol.2013.11.021.

[44] S. Sarkar, P. Pandya, K. Bhadra, Sequence specific binding of beta -carboline alkaloid harmalol with deoxyribonucleotides: binding heterogeneity, conformational, thermodynamic and cytotoxic aspects, PLoS One 9 (9) (2014) e0108022, https://doi.org/10.1371/journal.pone.0108022.

[45] S. Sarkar, P. Bhattacharjee, K. Bhadra, DNA binding and apoptotic induction ability of harmalol in HepG2: biophysical and biochemical approaches, Chem. Biol. Interact. 258 (2016) 142–152, https://doi.org/10.1016/j.cbi.2016.08.024.

[46] S. Sharma, M. Yadav, S.P. Gupta, K. Pandav, S. Kumar, Spectroscopic and structural studies on the interaction of an anticancer β–carboline alkaloid, harmine with gc and at specific DNA oligonucleotides, Chem. Biol. Interact. 260 (2016) 256–262, https://doi.org/10.1016/j.cbi.2016.08.025.

[47] S. Nafisi, Z.M. Malekabady, M.A. Khalilzadeh, Interaction of β-carboline alkaloids with RNA, DNA Cell Biol. 29 (12) (2010) 753–761, https://doi.org/10.1089/dna.2010.1087.

[48] P. Bhattacharjee, S. Sarkar, P. Pandya, K. Bhadra, Targeting different RNA motifs by beta carboline alkaloid, harmalol: a comparative photophysical, calorimetric and molecular docking approach, J. Biomol. Struct. Dyn. 34 (2016) 2722–2740, https://doi.org/10.1080/07391102.2015.1126694.

[49] P. Bhattacharjee, T. Ghosh, S. Sarkar, P. Pandya, K. Bhadra, Binding affinity and in vitro cytotoxicity of harmaline targeting different motifs of nucleic acids: an ultimate drug designing approach, J. Mol. Recogn. 31 (4) (2018) e2687, https://doi.org/10.1002/jmr.2687.

[50] M. Wickens, P. Anderson, R.J. Jackson, Life and death in the cytoplasm: messages from the 30 end, Curr. Opin. Genet. Dev. 7 (2) (1997) 220–232, https://doi.org/10.1016/s0959-437x(97)80132-3.

[51] M. Hossain, A. Kabir, G.S. Kumar, Binding of the phenothiazinium dye methylene blue with single stranded polyriboadenylic acid, Dyes Pigments 92 (3) (2012) 1376–1383, https://doi.org/10.1016/j.dyepig.2011.09.016.

[52] W.M. Scovell, Structural and conformational studies of polyriboadenylic acid in neutral and acid solution, Biopolymers 17 (4) (1978) 969–984, https://doi.org/10.1002/bip.1978.360170414.

[53] A.G. Petrovic, P.L. Polavarapu, Structural transitions in polyriboadenylic acid induced by the changes in pH and temperature: vibrational circular dichroism study in solution and film states, J. Phys. Chem. B 109 (49) (2005) 23698–23705, https://doi.org/10.1021/jp054280m.

[54] P. Giri, G.S. Kumar, Molecular aspects of small molecules-poly(A) interaction: an approach to RNA based drug design, Curr. Med. Chem. 16 (8) (2009) 965–987, https://doi.org/10.2174/092986709787581932.

[55] P. Giri, G.S. Kumar, Isoquinoline alkaloids and their binding with polyadenylic acid: potential basis of therapeutic action, Mini Rev. Med. Chem. 10 (2010) 568–577, https://doi.org/10.2174/138955710791384009.

[56] V. Brabec, O. Vrána, G.A. Platonova, E.M. Kogan, N.S. Sidorova, Biophysical studies of the modification of poly(rG). poly(rC) by cisplatin. Relations to the biological activity of the complex, Chem. Biol. Interact. 78 (1) (1991) 1–12, https://doi.org/10.1016/0009-2797(91)90098-r.

[57] R.E. Randall, S. Goodbourn, Interferons and viruses: an interplay between induction, signalling, antiviral responses and virus countermeasures, J. Gen. Virol. 89 (1) (2008) 1–47, https://doi.org/10.1099/vir.0.83391-0.

[58] E.V. Pilipenko, V.M. Blinov, V.I. Agol, Gross rearrangements within the 5'-untranslated region of the picornaviral genomes, Nucleic Acids Res. 18 (11) (1990) 3371–3375, 10.1093%2Fnar%2F18.11.3371.

[59] C.D. Kanakis, S. Nafisi, M. Rajabi, A. Shadaloi, P.A. Tarantilis, M.G. Polissiou, J. Bariyanga, H.A. Tajmir-Riahi, Structural analysis of DNA and RNA interactions with antioxidant flavonoids, Spectroscopy 23 (2009) 29–43, https://doi.org/10.3233/SPE-2009-0368.

[60] C.N. N'soukpoé-Kossi, A.A. Ouameur, T. Thomas, T.J. Thomas, H.A. Tajmir-Riahi, Interaction of tRNA with antitumor polyamine analogues, Biochem. Cell. Biol. 87 (4) (2009) 621–630, https://doi.org/10.1139/o09-036.

[61] A.A. Ouameur, P. Bourassa, H.A. Tajmir-Riahi, Probing tRNA interaction with biogenic polyamines, RNA 16 (10) (2010) 1968–1979, 10.1261%2Frna.1994310.

[62] K. Bhadra, M. Maiti, G.S. Kumar, Thermodynamics of the binding of cytotoxic protoberberine molecule coralyne to deoxyribonucleic acids, Biochim. Biophys. Acta Gen. Subj. 1780 (2008) 298–306, https://doi.org/10.1016/j.bbagen.2007.11.015.

[63] R. Sinha, M.M. Islam, K. Bhadra, G.S. Kumar, A. Banerjee, M. Maiti, The binding of DNA intercalating and groove binding compounds to A-form and protonated form of poly(rC).poly(rG): spectroscopic and viscometric study, Bioorg. Med. Chem. 14 (3) (2006) 800–814, https://doi.org/10.1016/j.bmc.2005.09.007.

[64] M.M. Islam, P. Pandya, S. Kumar, G.S. Kumar, RNA targeting through binding of small molecules: studies on t-RNA binding by the cytotoxic protoberberine alkaloid coralyne, Mol. Biosyst. 5 (3) (2009) 244–254, https://doi.org/10.1039/B816480K.

[65] J. Schauss, A. Kundu, B.P. Fingerhut, T. Elsaesser, Magnesium contact ions stabilize the tertiary structure of transfer RNA: electrostatics mapped by two-dimensional infrared spectra and theoretical simulations, J. Phys. Chem. B 125 (3) (2021) 740–747, https://doi.org/10.1021/acs.jpcb.0c08966.

[66] P. Bhattacharjee, S. Sarkar, T. Ghosh, K. Bhadra, Therapeutic potential of harmaline, a novel alkaloid, against cervical cancer cells in vitro: apoptotic induction and DNA interaction study, J. Appl. Biol. Biotechnol. 6 (4) (2018) 1–8, https://doi.org/10.7324/JABB.2018.60401.

[67] G.M. Morris, R. Huey, W. Lindstrom, M.F. Sanner, R.K. Belew, D.S. Goodsell, A.J. Olson, AutoDock4 and AutoDockTools 4: automated docking with selective receptor flexibility, J. Comput. Chem. 30 (6) (2009) 2785–2791, https://doi.org/10.1002/JCC.21256.

[68] C.W. Chan, D. Badong, R. Rajan, A. Mondragon, Crystal structures of an unmodified bacterial tRNA reveal intrinsic structural flexibility and plasticity as general properties of unbound tRNAs, RNA 26 (3) (2020) 278–289, https://doi.org/10.1261/rna.073478.119.

[69] D.S. Biovia, Discovery Studio Client (v20.1.0.19295, 2019.

[70] N. Gupta, P. Pandya, S. Verma, Computational predictions for multi-target drug design, Methods Pharmacol. Toxicol. (2019) 27–50, https://doi.org/10.1007/7653_2018_26.

[71] S. Kumar, P. Pandya, K. Pandav, S.P. Gupta, A. Chopra, Structural studies on ligand–DNA systems: a robust approach in drug design, J. Bio. Sci. 37 (3) (2012) 553–561, https://doi.org/10.1007/S12038-012-9212-8.

[72] J.C. Phillips, D.J. Hardy, J.D.C. Maia, J.E. Stone, J.V. Ribeiro, R.C. Bernardi, R. Buch, G. Fiorin, J. Hénin, W. Jiang, R. McGreevy, M.C.R. Melo, B.K. Radak, R. D. Skeel, A. Singharoy, Y. Wang, B. Roux, A. Aksimentiev, Z. Luthey-Schulten, E. Tajkhorshid, Scalable molecular dynamics on CPU and GPU architectures with NAMD, J. Chem. Phys. 153 (4) (2020) 044130, https://doi.org/10.1063/5.0014475.

[73] S. Jo, T. Kim, V.G. Iyer, W. Im, CHARMM-GUI: a web-based graphical user interface for CHARMM, J. Comput. Chem. 29 (11) (2008) 1859–1865, https://doi.org/10.1002/JCC.20945.

[74] P. Gopi, M. Gurnani, S. Singh, P. Sharma, P. Pandya, Structural aspects of SARS-CoV-2 mutations: implications to plausible infectivity with ACE-2 using computational modeling approach, J. Biomol. Struct. Dyn. (2022) 1–16, https://doi.org/10.1080/07391102.2022.2108901.

[75] P. Gopi, S. Singh, M.M. Islam, A. Yadav, N. Gupta, P. Pandya, Thermodynamic and structural profiles of multi-target binding of vinblastine in solution, J. Mol. Recogn. e2989 (2022), https://doi.org/10.1002/jmr.2989.

[76] S.I. Parvin, M.K. Mandal, P. Gopi, S. Singh, M.R. Khan, P. Pandya, M.M. Islam, H.A.R. Gazi, A comparative study on DNA and protein binding properties of thymol and thymoquinone, J. Biomol. Struct. Dyn. (2023) 1–13, https://doi.org/10.1080/07391102.2023.2180665.

[77] P. Sharma, P. Gopi, S. Singh, M.S.S. Rani, P. Pandya, Binding studies of sertraline hydrochloride with CT-DNA using experimental and computational techniques, Spectrochim. Acta: Mol. Biomol. Spectrosc. 300 (2023) 122910, https://doi.org/10.1016/J.SAA.2023.122910.

[78] K.W. Huang, C.Y. Wu, S.I. Toh, T.C. Liu, C.I. Tu, Y.H. Lin, Y.Y. Hsiao, Molecular insight into the specific enzymatic properties of TREX1 revealing the diverse functions in processing RNA and DNA/RNA hybrids, Nucleic Acids Res. 51 (21) (2023) 11927–11940, https://doi.org/10.1093/nar/gkad910.

[79] B. Ropii, M. Bethasari, I. Anshori, A.P. Koesoema, W. Shalannanda, A. Satriawan, R. Aditama, The assessment of molecular dynamics results of three-dimensional RNA aptamer structure prediction, PLoS One 18 (7) (2023) e0288684, https://doi.org/10.1371/journal.pone.0288684.

[80] D. Lessel, D.M. Zeitler, M.R. Reijnders, A. Kazantsev, F. Hassani Nia, A. Bartholomäus, H.J. Kreienkamp, Germline AGO2 mutations impair RNA interference and human neurological development, Nat. Commun. 11 (1) (2020) 5797, https://doi.org/10.1038/s41467-020-19572-5.

[81] A. Kumar, H. Vashisth, Conformational dynamics and energetics of viral RNA recognition by lab-evolved proteins, Phys. Chem. Chem. Phys. 23 (43) (2021) 24773–24779, https://doi.org/10.1039/D1CP03822B.
[82] W. Humphrey, A. Dalke, K. Schulten, VMD: visual molecular dynamics, J. Mol. Graph. 14 (1) (1996) 33–38, https://doi.org/10.1016/0263-7855(96)00018-5.
[83] B.J. Grant, A.P.C. Rodrigues, K.M. ElSawy, J.A. McCammon, L.S.D. Caves, Bio3d: an R package for the comparative analysis of protein structures, Bioinformatics 22 (21) (2006) 2695–2696, https://doi.org/10.1093/BIOINFORMATICS/BTL461.
[84] S.A. Bray, X. Lucas, A. Kumar, B.A. Grüning, The ChemicalToolbox: reproducible, user-friendly cheminformatics analysis on the Galaxy platform, J. Cheminf. 12 (1) (2020) 1–7, https://doi.org/10.1186/s13321-020-00442-7.
[85] K. Al-Khafaji, T. Taskin Tok, Amygdalin as multi-target anticancer drug against targets of cell division cycle: double docking and molecular dynamics simulation, J. Biomol. Struct. Dyn. 39 (6) (2021) 1965–1974, https://doi.org/10.1080/07391102.2020.1742792.
[86] P. Kumari, R.A. Poddar, Comparative multivariate analysis of nitrilase enzymes, Comput. Biol. Chem. 83 (2019), https://doi.org/10.1016/J.COMPBIOLCHEM.2019.107095.
[87] J. Chen, J. Wang, W. Zhu, Zinc ion-induced conformational changes in new Delphi metallo-β-lactamase 1 probed by molecular dynamics simulations and umbrella sampling, Phys. Chem. Chem. Phys. 19 (4) (2017) 3067–3075, https://doi.org/10.1039/C6CP08105C.
[88] S. Singh, P. Gopi, P. Pandya, Structural aspects of formetanate hydrochloride binding with human serum albumin using spectroscopic and molecular modeling techniques, Spectrochim. Acta: Mol. Biomol. Spectrosc. 281 (2022) 121618, https://doi.org/10.1016/j.saa.2022.121618.
[89] M.S. Valdés-Tresanco, M.E. Valdés-Tresanco, P.A. Valiente, E. Moreno, gmx_MMPBSA: a new tool to perform end-state free energy calculations with GROMACS, J. Chem. Theor. Comput. 17 (10) (2021) 6281–6291, https://doi.org/10.1021/acs.jctc.1c00645.
[90] J.B. Chaires, Competition dialysis: an assay to measure the structural selectivity of drug–nucleic acid interactions, Curr. Med. Chem. Anti Cancer Agents 5 (4) (2005) 339–352, https://doi.org/10.2174/1568011054222292.
[91] M.M. Islam, M. Chakraborty, P. Pandya, A.A. Masum, N. Gupta, S. Mukhopadhyay, Binding of DNA with Rhodamine B: spectroscopic and molecular modeling studies, Dyes Pigments 99 (2) (2013) 412–422, https://doi.org/10.1016/j.dyepig.2013.05.028.
[92] A.A. Masum, M. Chakraborty, P. Pandya, U.C. Halder, M.M. Islam, S. Mukhopadhyay, Thermodynamic study of rhodamine 123-calf thymus DNA interaction: determination of calorimetric enthalpy by optical melting study, J. Phys. Chem. B 118 (46) (2014) 13151–13161, https://doi.org/10.1021/jp509326r.
[93] M. Mohammad, I. Saha, K. Pal, P. Karmakar, P. Pandya, H.A.R. Gazi, M.M. Islam, A comparison on the biochemical activities of Fluorescein disodium, Rose Bengal and Rhodamine 101 in the light of DNA binding, antimicrobial and cytotoxic study, J. Biomol. Struct. Dyn. 40 (20) (2022) 9848–9859, https://doi.org/10.1080/07391102.2021.1936180.
[94] T. Antony, M. Atreyi, M.V.R. Rao, Interaction of methylene blue with transfer RNA – a spectroscopic study, Chem. Biol. Interact. 97 (1995) 199–214, https://doi.org/10.1016/0009-2797(95)03616-T.
[95] T. Hermann, Rational ligand design for RNA: the role of static structure and conformational flexibility in target recognition, Biochimie 84 (9) (2002) 869–875, https://doi.org/10.1016/s0300-9084(02)01460-8.
[96] M.M. Islam, R. Sinha, G.S. Kumar, RNA binding small molecules: studies on t-RNA binding by cytotoxic plant alkaloids berberine, palmatine and the comparison to ethidium, Biophys. Chem. 125 (2007) 508–520, https://doi.org/10.1016/j.bpc.2006.11.001.
[97] M.M. Islam, P. Pandya, S. Roy Chowdhury, S. Kumar, G.S. Kumar, Binding of DNA-binding alkaloids berberine and palmatine to tRNA and comparison to ethidium: spectroscopic and molecular modeling studies, J. Mol. Struct. 891 (2008) 498–507, https://doi.org/10.1016/j.molstruc.2008.04.043.
[98] B. Saha, G.S. Kumar, Spectroscopic and calorimetric investigations on the binding of phenazinium dyes safranine-O and phenosafranine to double stranded RNA polynucleotides, J. Photochem. Photobiol. B Biol. 161 (2016) 129–140, https://doi.org/10.1016/j.jphotobiol.2016.03.062.
[99] K. Bhadra, M. Maiti, G.S. Kumar, Interaction of isoquinoline alkaloid palmatine with deoxyribonucleic acids: binding heterogeneity, and conformational and thermodynamic aspects, Chem. Biodivers. 5 (2008) 575–590, https://doi.org/10.1002/cbdv.200890054.
[100] R. O'Brien, I. Haq, Applications of biocalorimetry: binding, stability and enzyme kinetics, in: J.E. Ladbury, M.L. Doyle (Eds.), Biocalorimetry 2, John Wiley & Sons, Ltd, 2005, pp. 1–34, https://doi.org/10.1002/0470011122.ch1.
[101] A.A. Saboury, M.S. Atri, M.H. Sanati, A.A. Moosavi-Movahedi, G.H. Hakimelahi, M.A. Sadeghi, Thermodynamic study on the interaction between magnesium ion and human growth hormone, Biopolymers 81 (2) (2006) 120–126, https://doi.org/10.1002/bip.20386.
[102] N.J. Buurma, I. Haq, Advances in the analysis of isothermal titration calorimetry data for ligand-DNA interactions, Methods 42 (2) (2007) 162–172, https://doi.org/10.1016/j.ymeth.2007.01.010.
[103] R. O'Brien, I. Haq, Applications of biocalorimetry: binding, stability and enzyme kinetics, in: J.E. Ladbury, M.L. Doyle (Eds.), Biocalorimetry 2, John Wiley & Sons, Ltd, 2005, pp. 1–34, https://doi.org/10.1002/0470011122.ch1.
[104] A.A. Saboury, M.S. Atri, M.H. Sanati, A.A. Moosavi-Movahedi, G.H. Hakimelahi, M.A. Sadeghi, Thermodynamic study on the interaction between magnesium ion and human growth hormone, Biopolymers 81 (2) (2006) 120–126, https://doi.org/10.1002/bip.20386.
[105] N.J. Buurma, I. Haq, Advances in the analysis of isothermal titration calorimetry data for ligand-DNA interactions, Methods 42 (2) (2007) 162–172, https://doi.org/10.1016/j.ymeth.2007.01.010.
[106] M. Khatun, G.C. Jana, S. Nayim, A. Dhal, A. Patra, M. Hossain, Evaluation of the size effect of hydrophobic ring substitution on 9-O position of berberine on DNA binding, J. Biomol. Struct. Dyn. (2023), https://doi.org/10.1080/07391102.2023.2180436.
[107] P. Karan, P. Panja, A. Khatun, J. Pal, S. Chakarabarti, S. Pal, A. Ghosh, M. Hossain, Synthesis of water-soluble novel bioactive pyridine-based azo coumarin derivative and competitive cytotoxicity, DNA binding, BSA binding study, and in silico analysis with coumarin, Bioorg. Chem. 138 (2023) 106532, https://doi.org/10.1016/j.bioorg.2023.106532.
[108] A. Das, K. Bhadra, G.S. Kumar, Targeting RNA by small molecules: comparative structural and thermodynamic aspects of aristololactam-β-D-glucoside and Daunomycin binding to tRNAphe, PLoS One 6 (8) (2011) e23186, https://doi.org/10.1371/journal.pone.0023186, 23197.
[109] F.V. Murphy, M.E. Churchill, Nonsequence-specific DNA recognition: a structural perspective, Structure 8 (4) (2000) R83–R89, https://doi.org/10.1016/S0969-2126(00)00126-X.
[110] J.H. Ha, R.S. Spolar, M.T. Record, Role of the hydrophobic effect in stability of site-specific protein–DNA complexes, J. Mol. Biol. 209 (4) (1989) 801–816, https://doi.org/10.1016/0022-2836(89)90608-6.
[111] J. Ren, T.C. Jenkins, J.B. Chaires, Energetics of DNA intercalation reactions, Biochemistry 39 (29) (2000) 8439–8447, https://doi.org/10.1021/bi000474a.
[112] M. Zgarbová, M. Otyepka, J. Sponer, F. Lankas, P. Jurecka, Base pair fraying in molecular dynamics simulations of DNA and RNA, J. Chem. Theor. Comput. 10 (8) (2014) 3177–3189, org/10.1021/ct500120v.
[113] N. Bhattarai, P. Baral, B.S. Gerstman, P.P. Chapagain, Structural and dynamical differences in the spike protein RBD in the SARS-CoV-2 variants B.1.1.7 and B.1.351, J. Phys. Chem. B 125 (26) (2021) 7101–7107, https://doi.org/10.1021/acs.jpcb.1c01626.
[114] J. Chen, J. Wang, W. Zhu, Zinc ion-induced conformational changes in new Delphi metallo-β-lactamase 1 probed by molecular dynamics simulations and umbrella sampling, Phys. Chem. Chem. Phys. 19 (4) (2017) 3067–3075, https://doi.org/10.1039/C6CP08105C.
[115] S. Konar, S.K. Sinha, S. Datta, P.K. Ghorai, The effect of ionic liquid on the structure of active site pocket and catalytic activity of a β-glucosidase from Halothermothrix orenii, J. Mol. Liq. 306 (2020) 112879, https://doi.org/10.1016/J.MOLLIQ.2020.112879.
[116] P.K. Parida, D. Paul, D. Chakravorty, The natural way forward: molecular dynamics simulation analysis of phytochemicals from Indian medicinal plants as potential inhibitors of SARS-CoV-2 targets, Phytother Res. 34 (12) (2020) 3420–3433, https://doi.org/10.1002/PTR.6868.
[117] S.S. Raghavan, S. Iqbal, N. Ayyadurai, K. Gunasekaran, Insights in the structural understanding of amyloidogenicity and mutation-led conformational dynamics of amyloid beta (Aβ) through molecular dynamics simulations and principal component analysis, J. Biomol. Struct. Dyn. 40 (12) (2021) 5577–5587, https://doi.org/10.1080/07391102.2021.1871955.
[118] P. Giri, G.S. Kumar, Molecular recognition of poly(A) targeting by protoberberine alkaloids: in vitro biophysical studies and biological perspectives, Mol. Biosyst. 6 (1) (2010) 81–88, https://doi.org/10.1039/b910706a.

[119] M.M. Islam, A. Basu, G.S. Kumar, Binding of 9-O-(ω-amino) alkylether analogues of the plant alkaloid berberine to poly(A): insights into self-structure induction, Med. Chem. Comm. 2 (7) (2011) 631–637, https://doi.org/10.1039/C0MD00209G.
[120] P. Paul, G.S. Kumar, Self-structure formation in polyadenylic acid by small molecules: new insights from the binding of planar dyes thionine and toluidine blue O, RSC Adv. 4 (49) (2014) 25666–25674, https://doi.org/10.1039/C4RA02671C.
[121] P. Paul, S.S. Maiti, S.C. Bhattacharya, G.S. Kumar, Spectroscopic, calorimetric, cyclic voltammetric and molecular modeling studies of new methylene blue-polyadenylic acid interaction and comparison to thionine and toluidine blue O: understanding self-structure formation by planar dyes, Dyes Pigments 136 (2017) 205–218, https://doi.org/10.1016/j.dyepig.2016.08.027.